Rotation Effects on Dynamics of Fluid Flow through Microchannels

by

Behnam Gheshlaghi

A thesis submitted to the Faculty of Graduate Studies and Research in partial fulfillment of the requirements for the degree of

Master of Science

Department of Mechanical Engineering

University of Alberta

Abstract

Effect of rotation on dynamcis of flow in microchannels is studied. In the frist study, an analytical solution is developed for the unsteady flow of fluid through a parallel rotating plate microchannel, under the influence of electrokinetic force using the Debye–Hückel (DH) approximation. Transient Navier-Stokes equations are solved exactly in terms of the cosine Fourier series by the separation of variables method. The effects of frame rotation frequency and electroosmotic force on the fluid velocity and the flow rate distributions are investigated. The rotating system is found to have a damped oscillatory behaviour. It is found that the period and the decay rate of the oscillations are independent of the DH parameter (κ). Furthermore, the rotation is shown to genearte a secondary flow and the ratio of flow in *y* and *x* directions is examined. It showed that both angular velocitiy and the Debye-Hückel parameters are influential on the induced transient secondary flow in the *y* direction. At high values for Debye-Hückel parameter and the roatation parameter the flow rates in *x* and *y* directions are found to be identical. In the second study, an analytical model is provided to describe the filling dynamics of a capillary filled with a viscous fluid containing spinning particles. The presence of spinning particles leads to making additional coefficients of viscosity, namely spin viscosity and vortex viscosity, which couples rotational and translational movements. Three different time stages have been noticed during the capillary filling phenomenon: inertia force dominated, visco-inertial, and viscous-dominated regions. The last two regions are found to be mainly affected by the spinning particles. An increase in the spin and vortex

viscosities increased the viscous force and thus reduced the front position of the moving liquid. The results of this study are validated using the no-angular-momentum (NAM) base-case results in literature and an excellent agreement was observed.

Keywords: Microfluidic channel, Electroosmotic, Rotating, Capillary, Spinning particles, SpinViscosity, Vortex viscosity.

Preface

In this thesis, different effects of rotations are theoretically studied by considering two main common subjects. Chapter 2 is published in the RSC Advances journal and Chapter 3 has been submitted to Journal of Colloid and Interface Science. I am the first author in both papers.

Chapter 2, Analytical Solution for Transient Electroosmotic Flow in a Rotating Microchannel, studies the effect of system rotation on the transient behavior of fluid flow in micro channels.

Chapter 3, Effect of spinning particles in the capillary filling dynamics of viscous fluids, considers the effects of conveyor rotation on the filling dynamics of fluid in micro channels.

I was responsible for the problem formulation and solution, and also the manuscript composition.

Dedication

I dedicate this dissertation to my parents, Shahla & Alireza. They have provided me with all the opportunities they could. They helped me understand the most important thing is being happy and healthy and anything else is an added bonus.

Acknowledgement

I would like to thank my supervisors, Dr. Mohtada Sadrzadeh and Dr. Aloke Kumar and my friends in Mechanical Engineering Department at the University of Alberta.

I wish them all success in their life and career.

Table of Contents

LIST OF TABLES

LIST OF FIGURES

LIST OF NOMENCLATURE

$\mathbf{b}$	Body force per unit volume.
C_n	Series solution constant.
e	Electron charge.
E	External electric field.
h	Half of the channel thickness.
k_B	Boltzmann constant
$m_{\pm}$	Mobility.
n_0	Bulk concentration of electrolytes in the liquid.
$n_{\pm}^*$	The concentration number of free charges in the fluid.
p	Pressure.
$Q_x(t)$	Transient flow rates in the *x* direction.
$Q_y(t)$	Transient flow rates in the *y* direction.
$\mathbf{u}^*$	Velocity vector.
u^*	Velocity in the *x* direction.
u	Non-dimensional velocity in the *x* direction.
v^*	Velocity in the *y* direction.
v	Non-dimensional velocity in the *y* direction.
$T(t)$	Temporal function.
t^*	Time.
t	Non-dimensional time.
$Z(z)$	Spatial function.

$\beta(t)$	Rotationally induced transient secondary flow in the y direction.
ε	Electric permittivity of the fluid.
κ^*	Debye–Hückel parameter.
κ	Non-dimensional Debye–Hückel parameter.
λ^2	Separation constant.
λ_D	Debye length.
μ	Viscosity of the fluid.
η'	Spin viscosity
ξ	The valence.
ζ	Vortex viscosity.
ρ	Fluid density.
ρ_e	Distribution of the net electric charge density near a charged surface.
$\boldsymbol{\tau}$	Extra stress tensor.
$\chi_1(z)$	Steady state component of the velocity profile.
$\chi_2(z)$	Transient component of the velocity profile.
ψ^*	Electric potential field.
$\psi(z)$	Non-dimensional electric potential field.
$\boldsymbol{\omega}$	Particle spinning rate
$\boldsymbol{\Omega}$	Angular velocity vector.

CHAPTER 1: **INTRODUCTION**

1.1.Background and Literature Review

Understanding liquid flow in small channels has been studied by many researchers over the years. It plays a huge role in the field of micro- and nanofluidics due to its different applications in microsystem technology [1] -[4] . The physical aspects of microfluidics are available in several comprehensive reviews and books [5] -[9] . The scaling laws that govern the balance of forces at the microscale are described in these references. Also, different properties of low Reynolds number flows (i.e. flows where viscosity dominates over inertia), capillarity, and electrokinetics are extensively discussed. These concepts are essential to understand the fluid behavior in complex geometries in microfluidic devices.

Microfluidic devices have the ability to perform precise manipulation for liquid handling capability at the Nano-liter scale. They have important features as precision, control, and reproducibility in experimentation which has made microfluidic devices an attractive platform for conducting different measurements. They are robust tools for realizing highly sensitive, high-throughput, and low-cost analysis. Size effect is the other important feature of microfluidics. It reveals unique physical properties of fluids on microchips. For example at microscale, the transfer distance of mass and heat and the reaction time is relatively small compared to those in happened in regular channel. Since the on-chip processes only require micro-scaled samples and reagents and since multiple sample processing steps can be completed on a single microchip,

microfluidics has established a revolutionary way for rapid and inexpensive detection in sophisticated chemical and biological analyses, while conventional techniques for these analyses were generally time- and money-consuming because of the complex processing procedures. In addition, microchips with multiple microchannels can be fabricated and being integrated with ultrasensitive detecting techniques to be used for multiplex analysis with high throughput and high sensitivity. Therefore, microfluidic analysis is known as a powerful tool for several sophisticated implementations in molecular biology and biomedicine, such as DNA sequencing and biomarker-screening for diseases [10] .

Characterizing flow through micro- and nano-channels is integral to the development of miniaturized biomedical diagnostic devices, commonly referred to as Lab-on-a-Chip (LOC) systems. LOC allows the integration of various components into a single micro-device. Microfluidics can be named as a key concept for LOC technology [11] . Although the fluid flow in micro channels is highly considered in different scientific aspects [12] -[20] however, the role of time in the flow behavior variations is not well established. Furthermore, fluid flow combined with rotational effects is an interesting issue which is not well studied. Here, we try to address two important parameters (i.e., time and rotation) on flow variations in micro-channels. Simple microchannel flow has been studied both experimentally and analytically [11] , revealed the relative importance of mechanisms such as slip, compressibility and acceleration.

Numerical techniques have been widely used for investigation of flow mechanism in microchannels instead of doing experiments. However, studies

about transient fluid flow are still very limited due to the high computational cost of properly resolved simulations. Sui and co-workers [22] and [23] investigated the fully-developed flow in a periodic wavy channel with rectangular cross-section for increasing Reynolds (Re) numbers ranging from the steady laminar to transitional flow regimes. They have reported that by increasing the Re, the flow transitioned from steady to time periodic with a single frequency, and subsequently to quasi-periodic flow with two distinct fundamental frequencies. Moreover, Zheng et al. [24] considered transient flow and heat transfer to study the transient, spatially non-periodic flow patterns in a semi-circular zigzag channel. Despite the existence of many simulation and analytical studies on the dynamic of fluid flow in micro channels, there are very few investigations on flow in microchannels in presence of centrifugal forces in the last few decades due to complexity of this area.

1.2.Rotating Microchannels

The recent advent of microfluidics has opened up the possibilities of using complicated bio-microfluidic arrangements on rotating platforms [25] . Their main advantages versatility in handling a wide variety of sample types, the ability to gate the flow of liquids, simple rotational motor requirements, large ranges of flow rates attainable, and the possibility of performing simultaneous and identical fluidic operations. A number of researches on distinctive aspects of centrifugally-aided microchannel flows leads to the common consensus that an artificial gravity is induced by rotational effects which can pump the fluid in the radial direction.

One of the first theoretical studies was presented by Takashima [26] who examined the effect of rotation in a dielectric fluid confined between two parallel plates under the action of an AC electric field by neglecting centrifugal force. Chang and Wang [27] investigated the rotating EO flow over an infinite plate and also in a channel formed by two parallel plates. They applied the Debye-Huckel approximation for charge distributions. They have shown that the rotational speed is the most important parameter affecting the flow behavior for the single plate case. However, for the microchannel case, the electrokinetic width is also an influential parameter on the flow characteristics. The impact of rotation is found to reduce the axial flow rate along the direction of the applied electric field. Furthermore, it induced a secondary transverse flow. They also showed that the location of maximum velocity shifted towards the boundary with increasing the rotation speed. Xie and Jian [28] numerically studied the rotating electro-osmotic flow of power-law fluids in a slit micro-channel in the presence of high zeta potential. The electric double layer (EDL) potential distribution was considered by using nonlinear Poisson–Boltzmann equation. Finite difference method was used to compute the velocity profiles of the Non-Newtonian fluid numerically. They reported the influences of the flow behavior index, the rotating angular velocity, the wall zeta potential, and the electrodynamic width on the velocity profiles. Detailed theoretical models was developed by Kim and Kwon [29] who considered the centrifugal force in the capillary filling without considering the surface tension effects. Also, Ducrée et al. [30] and Brenner et al. [31] showed the

influence of Coriolis effects on enhancing the extent of microfluidic mixing in high speed rotationally-aided microchannel flows.

1.3. Electro-osmotic flow in micro channels

It is well known that electro-osmotic flow (EOF) is an alternative process of transporting fluids induced by an applied electric field. Some of above mentioned operations in the microfluidic devices require pumping, controlling and manipulating sample volumes. Electroosmotic flow (EOF) has frequently been used for manipulating and controlling liquid flows in micro-devices [32] . It refers to liquid flow induced by an applied external electric field along electrostatically charged surfaces [33] . In the theory of electrokinetic, a charged surface brought into contact with an electrolyte solution. Therefore, the electrolyte counter ions move towards the charged surface and they constitute a layer with a high concentration of counter ions. An electric diffuse double layer (EDL) near the charge surface is created due to presence of mobile counter ion layer and the immobile surface charge layer. In order to make a net migration, an external electric field is applied along the surface. This leads to a force applied on the ions within the mobile diffuse electric layer. Thus, the ions in the mobile part of the EDL undergo a net migration in the opposite direction and carry the liquid along with them. It causes the movement of the liquid [34] .

There are many studies conducted on the theoretical examination of the EOF characteristics in microchannels [35] -[39] . These studies have been applied

to different microfluidic applications. For example, as an application for pumping, Arulanandam et al. [40] investigated characteristics of electroosmotic flow in rectangular microchannels. They used a 2D Poisson–Boltzmann equation and the 2D momentum equation to show the significant influence of the channel cross-section geometry on the velocity field and the volumetric flow rate. They also examined the effect of the ionic concentration on the velocity field and the volumetric flow rate. Wu et al. [41] carried out a systematic 3-D numerical simulations to examine the effect of zeta potential on the sample separation. Their Theoretical simulation results showed that zeta potential distribution controls the sample band broadening and manipulates sample separation efficiency. In other study [42] , an analytical solution is presented for the transient electroosmotic flow of non-Newtonian fluids in square cross-section microchannels. The authors obtained a hyperbolic partial differential equation and they used the Green's functions for the steady-state regime and the method of separation of variables for the transient state. They have shown that the relaxation time parameter affects the flow oscillatory behavior. Chang [43] considered transient electro-osmotic flow through a cylindrical microcapillary containing a salt-free medium. Both surface charge density and surface potential are assumed to be constant. The nonlinear Poisson-Boltzmann equation was solved to yield the exact analytical solutions for the electric potential distribution and the transient electro-osmotic flow velocity. Their results showed that there is similarity between transient behavior of EOF in a cylindrical tube and the same flow in a microchannel containing an electrolyte solution. On the other hand, the steady-state electro-osmotic flow significantly

deviates from the typical plug flow at higher surface charge. Keh and Tseng [44] studied the transient response of electrolyte solutions in a narrow capillary tube or slit. The external stimulation was a step change in the applied electric field and/or pressure gradient. They obtained closed-form formulas for the transient flow rate, electro-osmotic velocity, and electric current. The have also shown that the behavior of the transient electrokinetic flow in a capillary tube and in a capillary slit are similar. However, they found faster rate of evolution of the flow in a tube than that in a slit having half thickness equal to the tube radius. They showed that for small electric oscillating Reynolds number and high electrokinetic width the electro-osmotic velocity amplitude shows a square plug like profile. Burgreen and Nakache [45] formulated the mathematical model for electroosmotic flow in an ultrafine slit.

In some numerical studies [45] -[47] , the electroosmotic flow was simulated at the intersection of a cross-microchannel during a chemical-sample injection procedure. Bianchi et al. [47] showed that the velocity distribution of flow at a microscale T-junction intersection is affected by the relative zeta potentials and channel widths. Therefore, the linear approximation of the Poisson–Boltzmann equation for large zeta potential still can predict the plug velocity accurately. Ajdari [48] demonstrated the generation of vortices in electro-osmosis with sinusoidal surface potential in micro-channel. In a theoretical study, Takashima [26] examined the effect of rotation in a dielectric fluid confined between two parallel plates under the action of an AC electric field by neglecting centrifugal force.

There are also some studies on the transient electroosmotic flows. Zhao et al. [49] obtained an analytical solution for the unsteady electroosmotic flow of Oldroyd-B fluids. They reported that an oscillatory behavior around the terminal velocity is because of the relaxation time and retardation time effects. Li et at. [50] examined transient electroosmotic flows of non-Newtonian fluids in a microchannel and showed that higher normalized relaxation time leads to longer time for flow to attain the steady state.

1.4.Capillary filling

Capillary filling is the ability of a liquid to fill a narrow space without the assistance of external forces such as gravity. Capillary filling dynamics has a wide range of applications from in lab-on-a-chip based micro–total analysis systems [6] to the transport of biological fluids in flora and fauna[51] . Over the years, numerous studies have been reported on the capillary filling dynamics of various fluids, which include analytical and semi-analytical as well as experimental investigations [52] -[55] . Lucas and Washburn [52] and [53] are the pioneer researchers in this area. As a basic model governing the transients of the capillary filling and meniscus advancement, they concluded that the interplay between the driving surface tension forces and the resistive viscous forces results in the filling length. According to their studies, the filling length is proportional to the square root of the filling time [53] -[61] . The flow regime in this region is called Washburn regime.

Studies on the early (inertial) regimes of capillary filling show that there is a linear regime prior to Washburn regime. In this regime, capillary forces and the inertial forces balance each other [62] -[66] . Quere [56] has also reported the linear variations experimentally. Independent of the channel orientation, researchers have demonstrated that the linear regime at the initial stages of capillary filling is universal. The strength of viscous force determines the regime at which the liquid front can enter (i.e., either the Washburn or an oscillatory regime) [56] . Recently, the effects of entrance pressure and unsteady flow effects have been studied, extending the application of the lumped model approach [67] . Although such models cannot capture the meniscus shape explicitly, their predictions have been shown to agree well with experiments [68] -[70] .

The main reason for the rotation-translation coupling [71] in molecular fluids is the presence of non-symmetric pressure tensor which appears when there are non-central forces. It makes additional coefficients of viscosity that are called spin and vortex viscosity. Dahler and Scriven [72] derived the governing equations describing the dynamics of such fluids by considering the spin velocity of the particles. It is important to notice that this velocity is not necessarily one-half the vorticity or the rotation rate of the fluid. So there is a difference between them and it causes an antisymmetric portion in the stress. This quantifies a tensor quantity called the vortex viscosity [73] and[74] . For a dilute suspension it can be estimated properly [75] . Condiff and Dahler [76] used the antisymmetric stress and generalized Navier-Stokes equations for the velocity and spin fields to describe the interaction of internal spin with fluid flow. They assigned continues

spin field to the rotation of the molecular subunits. They also introduced the vortex viscosity. In other work [77] vortex viscosity was used to examine the behavior of ferromagnetic suspension in a uniform rotating magnetic field. They used the coupling of rotational and translational motions of molecules to obtain a pumping mechanism. The rotation of the applied field led to the motion (pumping) of the medium.

The purpose of this study is to take into account different effects of rotation on the behavior of fluid flow in two different systems. First a rotating system is considered in which a transient fluid flow is theoretically studied. The effects of angular velocity and the DH parameter on the dynamics of fluid flow are studied. Next, the capillary filling dynamics of fluid in microchannels is investigated. The effects of spin viscosity and vortex viscosity on the fluid flow have been examined.

1.5.Objectives

The main goals of this thesis are (i) to study the effects of channel rotation on the dynamics of viscous fluids and (ii) to study the effects of rotating particles on the capillary filling dynamics.

In the first phase of this study the effect of centrifugal force induced by rotation is taken into account in the Navier-stokes equations. Then the transient equations are solved exactly. The effect of electroosmotic force is also considered

in analysis. Then we have investigated the effect of various parameters on velocity and flow rate.

In the second part, the capillary filling dynamics is modeled to predict the front end position of the fluid with spinning particles. Our numerical results are in good agreement with the previously published data about the effects of viscosities on the front end position of fluid.

1.6.Thesis Outline

Chapter 1 of the thesis provides a brief introduction about microfluidic and effects of rotation on fluid behavior. In this chapter, the theoretical background of electroosmotic and capillary flow is discussed and the papers related to fluid flow in microchannels and capillary flow are reviewed.

In the second chapter, an analytical solution has been presented for the unsteady flow of fluid through a parallel rotating plate microchannel, under the influence of electrokinetic force using the Debye–Hückel (DH) approximation. We have exactly solved the transient Navier-stokes equations to find the velocities and flow rates in terms of DH parameter (κ) and the rotation frequency.

In Chapter 3, an analytical model is presented to describe the filling dynamics of a capillary by a viscous fluid with spinning particles. Spinning particles in the viscous fluid make additional coefficients of viscosity called spin and vortex viscosities. Here, the fluid penetration in capillary is identified based on a coupling between rotational and translational movements. The variation of

the viscous force and fluid front position as a function of time is invedtigated for different vortex viscosity and spin viscosity.

In Chapter 4 the major findings of this work has been summarized. Based on the outcome of this work, recommendations are provided for further development in this field.

CHAPTER 2: **Analytical Solution for Transient Electroosmotic Flow in a Rotating Microchannel**

2.1. Introduction

Flows through microchannel has become one of the most important research areas in recent years due to the unique phenomena occurring in micro scale level such as development of thin electric diffuse layer, called electrical double layer (EDL) [71] -[76] . The thickness of the EDL layer is comparable with size of the microchannel so that the length scales of electrostatic interactions enables the development of many high-impact technologies in the area of electrokinetic transport in microchannels. In such technologies, the electroosmotic flow (EOF) is the prevalent phenomenon for transport of small volumes of aqueous solutions when an electric field is applied across a microchannel with charged wall [77] . The electrical forces on the EDL near the interface of a solid surface and an electrolyte solution generates a fluid flow [78] and [79] .

The characteristic of EOF in microchannels is typically examined by solving continuity and momentum equations in the presence of an electrical body force given by Poisson-Boltzmann (PB) equation. These equations have been analytically solved for various geometries, flow properties and electrolyte solution characteristics using Debye-Hückel (DH) approximation [73] [1–9]-[81] . This approximation can be used for small magnitude of wall zeta-potential (<0.025 V) which makes the PB equation

linear, thus leading to an analytical and explicit expression of potential profile.

Levine *et al*. [85] analytically solved the steady state problem of an electrokinetic flow in a fine cylindrical capillary considering the DH approximation. This study provided more precise calculation of power requirements for pumping electrolytes through fine capillaries. Burgreen and Nakache [45] analytically studied electrokinetic laminar steady flow in a very thin rectangular channel without DH approximation. Their analysis provided a solution for the case of high ionic energy and small electrokinetic radius. Hsu *et al*. [86] theoretically studied flow of an electrolyte solution through an elliptical microchannel to simulate the flow of a fluid in vein. They considered a time independent spatial variation for the liquid velocity with different types of boundary conditions on the channel wall. In their analysis, they didn't consider any assumption regarding the thickness of the double layer and the level of the electrical potential in order to present a more realistic description for biological systems. They also reported that the effects of boundary conditions are more apparent when the size of microchannel decreases. The EOF in human meridian was studied by Sheu *et al*. [87] thorough a numerical model considering a steady state creeping flow for a tissue fluids motion. The tissue fluids contain ions and nutrition and they interact with the blood in the capillary vessel through a complex nonlinear electro-osmosis transport process. EOF in microchannels in presence of thermal effects has also

attracted many attentions. Chen [78] presented analytical expressions for the velocity and the temperature distributions of a fully-developed non-Newtonian fluid flow in a microchannel subject to heat flux at boundary conditions. Das and Chakraborty [88] obtained closed form expressions for velocity and temperature distribution of steady and fully developed flow of power-law fluid. They examined the effect of non-Newtonian parameters on flow behaviour.

In all the above mentioned studies, electrokinetic (more specifically EOF) was applied as the only mean for controlling the flow of liquids in microfluidic channels [82] . Plug-like velocity profile along with easy controllability is the main characteristics the EOF in microchannels. However, the electrokinetic pumping suffers from drawbacks that have directed researches toward techniques for generating secondary flow. First, physicochemical properties, such as ionic strength and pH, may affect the pumping performance. For example, excessive Joule heating (the process by which the passage of an electric current through a conductor releases heat) prohibits pumping of the liquids with high ionic strength [83] . Therefore, it may be difficult or impossible to use EOF to pump biological fluids, such as blood and urine [71] . Second, electrokinetic pumping requires high-voltage supplies which may have adverse safety effects. Third, electrokinetic pumping works for fluids without any trapped bubbles in the microchannels. Finally, due to Joule heating, EOF cannot be used for high flow rates (>1 μL/s) in wide channels (>1 μm) [84] . A simple and safe

alternative for controlling the flow of liquids in microfluidic channels is based on centrifugal force which is not sensitive to the chemical properties of the liquid. This system can also be applied for liquids with trapped bubbles and a wide range of channel sizes. In a centrifugal system, the fluid spatial and temporal controls have to be incorporated over the position of fluids in micro-channels.

Duffy et al. [89] conducted experimental investigation on the effect of centrifugal force on the micro-flow transport through microscopic channels fabricated in a plastic disk. The fluid was pumped outward by centrifugal force due to the rotation of the disk at 60-3000 rpm. They applied this method to pump biological fluids, such as blood and urine, since the driving force for fluid flow was no longer sensitive to physicochemical properties of fluids such as pH and ionic strength. Chang and Wang [27] investigated steady state rotating EOF over an infinite plate and inside a rectangular channel using the DH approximation for charge distributions. They have shown that, the speed of rotation and the electrokinetic width are the most important parameters affecting the steady flow in a microchannel. In addition, they have demonstrated that when the speed of rotation increases, axial and transverse flows vanish and the entire system forms a rigid body rotation. Xie and Jian [28] analysed the rotating EOF of power-law fluids at high zeta potentials in a microchannel. They applied the nonlinear PB equation for the EDL potential distribution. Using the finite difference method, they have numerically computed the rotating EOF velocity profiles

for non-Newtonian fluids. However, the velocity profiles in their study are only computed at the steady-state condition. Li et. al [39] continued this study for the third grade fluids. They used the perturbation method to approximately obtain the solutions by assuming a slight non-Newtonian behaviour. Recently, Ng and Qi [90] presented a more detailed study on the electro-osmotic flow in rotating rectangular microchannels. They considered the same steady state problem as in Ref [27] to represent the effect of channel width, different combination of wall's charge on the , Ekman-EDL, flow structure and flow rate.

In this study an analytical solution is developed for the transient electroosmotic flow in a rotating microchannel. To the best of authors' knowledge, this time dependent behaviour has not been reported in an exact closed-form series solution. First, a general solution of the problem is obtained via superposition and separation of variables techniques. By using a cosine Fourier series expansion, the governing complex partial differential equation (PDE) was solved to yield a closed-form solution. Next, the analytical solutions for velocity and flow rate were applied to some examples. Structures of boundary layer at higher rotational frequencies are studied and the rotational induced secondary flows are discussed. Moreover, transient secondary flow in the y direction is shown to be dependent on angular velocity and the Debye-Hückel parameters. Finally, the analytical solution results were compared with numerical solutions from MATHEMATICA and previously published results.

2.2. Problem formulation

The geometry for the present analysis is shown in Figure. 2.1. It consists of two parallel plates separated by a distance $2h$. The bottom and the top plate are located at z=-h and z=h, respectively.

The basic field equations governing the flow of an incompressible fluid between two parallel walls of a microchannel are the continuity equation and the modified Cauchy equations given by

$$\nabla.\mathbf{u}^* = 0, \tag{2.1.a}$$

$$\rho\left(\frac{\partial \mathbf{u}^*}{\partial t^*} + \mathbf{u}^*.\nabla\mathbf{u}^* + 2\boldsymbol{\Omega}\times\mathbf{u}^*\right) = -\nabla p + \nabla.\boldsymbol{\tau} + \mathbf{b}, \tag{2.1.b}$$

where $\mathbf{u}^* = (u^*, v^*, 0)$ is the velocity vector, ρ is the incompressible fluid density, t^* is the time, $\boldsymbol{\Omega} = (0,0,\Omega)$ is the angular velocity vector, p is the modified pressure including centrifugal force ($p = P - \rho/2\ |\boldsymbol{\Omega}\times\mathbf{r}\ |\text{^}2$), $\boldsymbol{\tau}$ is the extra stress tensor, and $\mathbf{b}$ is the body force per unit volume. The pressure gradient along the microchannel is assumed to be zero except for the centrifugal force that is included in the modified pressure. In the EO flow (except for electrophoresis applications with high electric field [91]) the Reynolds number is less than a unity which results in negligible convective term in NS equation ($\mathbf{u}^*.\nabla\mathbf{u}^* = \mathbf{0}$) [92] . List of constants and parameters used here is presented in Table 1.

Table 2-1: Constants and parameters

Parameter	**Value**
electron charge, e	1.6×10^{-19} C
Boltzmann Constant, k_B	1.38×10^{-23} J K^{-1}

Avogadro number, N_A	6.022×10^{-23} mol^{-1}
electric permittivity, ε	695×10^{-12} F m^{-1}
molar conductivity, σ_M	$(151.9 - 143.36) \times 10^{-4}$S m^2 mol^{-1}
electric field strength, E	10^4 V m^{-1}
molar concentration	$10^{-5} - 10^{-2}$ mol L^{-1}
wall electric potential, ψ	10 mV
Electric field strength,E	10^4 V m^{-1}
absolute temperature, T	293 K
dynamic viscosity, μ	10^{-3} Pa s
density, ρ	10^3 kg m^{-3}
channel width, $2h$	200 μm

To find the electric potential distribution within the EDL the Poisson-Nernst-Plank (PNP) model is considered. The species conservation equation can be written as:

$$\frac{\partial n_{\pm}^*}{\partial t^*} = -\nabla.\left(\mp e m_{\pm} \pm n_{\pm}^* \nabla\psi^* - m_{\pm} k_B T \nabla n_{\pm}^*\right), \tag{2.2}$$

where n_+^* and n_-^* are the concentration number of free charges in the fluid, e is the elementary charge, $m_{\pm}$ is the mobility, ψ^* is the electric potential in the fluid, k_B is the Boltzmann constant, and T is the absolute temperature. By subtracting the positive and negative number concentrations the following equation is obtained:

$$\frac{\partial \rho_f^*}{\partial t^*} = -\nabla.\left(\sigma \nabla \psi^* - D \nabla \rho_f^*\right), \tag{2.3}$$

with $\rho_f^* = e(n_+^* - n_-^*)$ and $\sigma = e(m_+^* n_+^* - m_-^* n_-^*)$. The electric conductivity of electrolyte (σ) is found based on the molar conductivity of solution[10], $\sigma = 1000 M \sigma_M$. Substituting Eq. (3) into Eq.(2) yields [34] :

$$\frac{\tau_c}{\tau_p}\frac{\partial \rho_f^*}{\partial t^*} = -\nabla.\left(\nabla \psi^* - \frac{\varepsilon D}{\sigma h^2}\nabla \rho_f^*\right), \tag{2.4}$$

where ε is the electric permittivity and $\tau_c = \varepsilon/\sigma$ and $\tau_p = \mu h^2/\varepsilon \psi^{*2}$ are the charge relaxation time scale and the process time scale, respectively. Here, based on the parameters presented in the Table 1, the process time is higher than charge relaxation time ($\tau_p \gg \tau_c$), the dynamics of charges becomes negligible compared to the fluid motion and the PNP equation simplifies to the Poisson-Boltzmann equation. The net electric charge density in the fluid and the electric potential field $\psi^*(z)$ within the EDL are related as follows (see appendix):

$$\frac{\partial^2 \psi^*(z^*)}{\partial z^{*2}} = -\frac{\rho_e}{\varepsilon}. \tag{2.5}$$

The term, ρ_e is the Boltzmann distribution of the net electric charge density near to the charged walls described as [93]

$$\rho_e = -2 n_0 e \xi \sinh\left(\frac{e\xi}{k_B T}\psi^*\right), \tag{2.6}$$

where n_0 is the bulk concentration of electrolytes in the liquid ($n_0 = 1000 N_A M$), e is the electron charge, and ξ (=1) is the valence. The body force per unit volume, defined in Eq.(1.b) can be written as $\mathbf{b} = (\rho_e E, 0, 0)$.

It is assumed that the electrical potential is small compared with the thermal energy of the charged species. Hence, the DH linearization principle ($\sinh(A) \approx A$) [34] can be applied to obtain the following simpler linear relation:

$$\frac{\partial^2 \psi^*(z^*)}{\partial z^{*2}} = \kappa^{*2}\psi^*(z^*), \tag{2.7}$$

where $\kappa^* = \sqrt{2n_0 e^2 \xi^2 / \varepsilon k_B T}$ is the DH parameter and it is the inverse of the Debye length (λ_D). This approximation can be used when the Debye thickness is small but finite, i.e., for $10 \leq h/\lambda_D \leq 10^3$Error! Reference source not found. [94] .

Scaling factors are defined to simplify the analysis procedure as follows:

$$z = \kappa^* z^*, \psi = \frac{\psi^*}{\zeta}, u = \frac{\mu}{\zeta \varepsilon E} u^*, v = \frac{\mu}{\zeta \varepsilon E} v^*, t = \frac{\mu}{h^2 \rho} t^*??, \ \kappa = h\kappa^*. \tag{2.8}$$

Applying these scaling factors to Eqs. (2.1.b) and (2.7) along with considering the no-slip (zero velocities) boundary condition on the channel walls, the following dimensionless governing equations are obtained in x and y directions:

$$\frac{\partial u}{\partial t} - \frac{\partial^2 u}{\partial z^2} - 2\omega v - \frac{\partial^2 \psi}{\partial z^2} = 0, \tag{2.9.a}$$

$$\frac{\partial v}{\partial t} - \frac{\partial^2 v}{\partial z^2} + 2\omega u = 0, \tag{2.9.b}$$

where $\omega = \rho\Omega/\mu\kappa^2$ is the dimensionless angular velocity. In the Electrokinetic part, one can solve the dimensionless form of Eq. (2.7) subjected to the boundary conditions of $\psi(\pm 1) = 1$ as follows:

$$\psi(z) = \frac{\cosh(\kappa z)}{\cosh(\kappa)}. \tag{2.10}$$

To facilitate solutions of Eqs. (2.9.a) and (2.9.b), a complex function of $\chi(z,t) = u(z,t) + \mathrm{i}v(z,t)$ with $\mathrm{i} = \sqrt{-1}$ was used. Hence, the hydrodynamic equations (Eqs. (2.9.a and b) can be written as a single complex partial differential equation as follows:

$$\frac{\partial^2 \chi}{\partial z^2} - \frac{\partial \chi}{\partial t} - 2\mathrm{i}\omega\chi + \frac{\partial^2 \psi}{\partial z^2} = 0. \tag{2.11}$$

2.3. Solution procedure

To find 'analytical' solution of complex PDE described in Eq. (2.11), the superposition property is used:

where, $\chi_1(z)$ is the steady state component of the velocity profile and $\chi_2(z,t)$ is the transient component. Introducing Eq. (2.12) into Eq. (2.11) while imposing the boundary and initial conditions, the following set of differential equations are obtained for $\chi_1(z)$:

$$\frac{\partial^2 \chi_1}{\partial z^2} - 2i\omega\chi_1 + \frac{\partial^2 \psi}{\partial z^2} = 0, \text{ with } \quad \chi_1(1) = 0, \quad \chi_1(-1) = 0, \tag{2.13}$$

and for $\chi_2(z,t)$

$$\frac{\partial^2 \chi_2}{\partial z^2} - \frac{\partial \chi_2}{\partial t} - 2i\omega\chi_2 = 0, \text{ with } \chi_2(1,t) = 0, \ \chi_2(-1,t) = 0, \tag{2.14}$$

$$\chi_2(z,0) = -\chi_2(z).$$

Applying the corresponding boundary conditions to the differential equation Eq.(2.13), yields the steady state component of the velocity profile as [27] follows:

$$\chi_1(z) = \frac{\kappa^2\left[\frac{\cosh(\sqrt{2i\omega}z)}{\cosh(\sqrt{2i\omega})} - \cosh(\kappa z)\,\mathrm{sech}(\kappa)\right]}{(\kappa^2 - 2i\omega)}. \tag{2.15}$$

Eq. (2.14) is solved using the separation of variables method by assuming $\chi_2(z,t) = Z(z)T(t)$, with $Z(z)$ and $T(t)$ being the spatial and temporal functions, respectively.

The new form for $\chi_2(z,t)$ is substituted into equation (2.14) to obtain the following separated ordinary differential equations (ODEs) for z and t:

$$\frac{1}{Z(z)}\frac{\partial^2 Z(z)}{\partial z^2} = \frac{1}{T(t)}\frac{\partial T(t)}{\partial t} + 2i\omega = -\lambda^2 \tag{2.16}$$

where, λ^2 is the separation constant.

A solution of Eq. (2.16) for $Z(z)$ satisfying its boundary conditions $Z(1) = Z(-1) = 0$ can be assumed in the form $Z(z) = \cos(\lambda_n z)$ with $\lambda_n = (2n+1)\pi/2$. Also, the exact solution for $T(t)$ in Eq. (2.16) is as follows:

$$T(t) = C_n e^{-(\lambda_n^2 + 2i\omega)t}, \tag{2.17}$$

where C_n is a constant. Hence the expression for $\chi_2(z,t)$ becomes:

$$\chi_2(z,t) = \sum_{n=0}^{\infty} C_n \cos(\lambda_n z) e^{-(\lambda_n^2 + 2i\omega)t}. \tag{2.18}$$

Next, the initial condition requires $\chi_2(z,0) = -\chi_1(z)$ and the coefficient C_n is determined as

$$\mathrm{C_n} = -\left[\frac{16\kappa^2(1+2n)\pi\cos(n\pi)}{(4\kappa^2 + (2n\pi+\pi)^2)(8i\omega + (2n\pi+\pi)^2)}\right].$$

Finally, the solution for $\chi(z,t)$ is:

$$\chi(z,t) = \frac{\kappa^2\left[\frac{\cosh(\sqrt{2i\omega}z)}{\cosh(\sqrt{2i\omega})} - \cosh(\kappa z)\,\mathrm{sech}(\kappa)\right]}{(\kappa^2 - 2i\omega)} + \sum_{n=0}^{\infty} A_n e^{-\left[2i\omega + \left(\frac{2n+1}{2}\pi\right)^2\right]t}, \tag{2.19}$$

$$A_n = -\left[\frac{16\kappa^2(1+2n)\pi\cos(n\pi)}{(4\kappa^2+(2n\pi+\pi)^2)(8i\omega+(2n\pi+\pi)^2)}\right]\cos\left(\frac{2n+1}{2}\pi z\right).$$

Integrating Eq. (2.19) with respect to z leads to the following expression for the normalized complex volume flow rate per width:

$$Q(t) = Q_x(t) + iQ_y(t) = \int_{-1}^{1}\chi(z,t)dz = \frac{\left[\frac{2\kappa^2\tanh(\sqrt{2i\omega})}{\sqrt{2i\omega}} - 2\kappa\tanh(\kappa)\right]}{(\kappa^2 - 2i\omega)} + \tag{2.20}$$

$$\sum_{n=0}^{\infty}\left\{-\left[\frac{64\kappa^2\mathrm{Cos}^2(n\pi)}{(4\kappa^2+(2n\pi+\pi)^2)(8i\omega+(2n\pi+\pi)^2)}\right]e^{-\left[2i\omega+\left(\frac{2n+1}{2}\pi\right)^2\right]t}\right\},$$

Terms, $Q_x(t)$ and $Q_y(t)$ are the transient flow rates in the x and y direction, respectively. Finally, $\beta(t) = \tan^{-1}\left[Q_y(t)/Q_x(t)\right]$ is defined as a parameter representing the rotationally induced transient secondary flow in the y direction.

The solution represented in Eq. (2.19) goes through three stages of development. Firstly, when$\omega t \ll 1$, the Coriolis force in the momentum Eq. (2.9) is small compared to the stress gradient. Using the relationship $e^{i\omega t} = \cos(\omega t) + i\sin(\omega t)$ at this stage, Eq. (2.19) is re-written as follows:

$$\chi(z,t) = \chi_1(z) + \sum_{n=0}^{\infty}\left\{C_n\cos(\lambda_n z)\,e^{-\lambda_n^2 t}\right\}. \tag{2.21}$$

At this stage, the solution is related to a non-rotating transport accelerated by a constant stress. Next, at longer times, the Coriolis force deflects the flow towards the steady-state condition. The solution undergoes damped

inertial oscillations near to the steady-state condition. Finally, after a long time, for $\omega t \gg 1$ momentum completely diffuses to the microchannel flow. At this stage, velocity field in the microchannel is at the final phase of inertial oscillations, which are damped by the viscous stress gradient. Therefore, the inertial oscillations are dissipated and one may use the first unsteady term of solution in Eq. (2.19) for long time solution, as represented in literature [27] .

2.4. Results and Discussion

To illustrate the nature and general behavior of the analytical solution, some numerical examples are considered in this section. The variation of the dimensionless velocity field ($u(z,t)$) as a function of time for different values of DH parameter (κ) and dimensionless angular velocity (ω) are discussed using contour plots. Then, the effects of κ and ω on the evolution of rotationally induced secondary flow in the y direction are investigated by examining $\beta(t)$. The fluid experiences a force imparted due to EOF and the frame rotation influences the flow velocity field with centrifugal force. In order to find the overall transient signature of the flow both of these two factors and their relative strength must be included. However, we note that the oscillation characteristic of flow, is properly described by the rotation parameter (ω), apart from the DH parameter (κ). In all the numerical results, the truncation constant of $n = 5$ was found to yield satisfactory results.

2-D dimensionless contour plot of velocity evolution (x-component, $u(z,t)$) and the centre-line velocity profile versus time are shown in Fig. 2.2. To investigate the influence of rotation, different values for the dimensionless rotation parameter $\omega = 1.0, 2.5, 5.0, 10 \text{ and } 20$ are used. The transient centre-line velocity is also plotted to have a better comparison of velocity magnitude and behaviour at the centre of channel at various ω values. In all these figures, the horizontal axis is the dimensionless time parameter ($0 < t < 3$).

Results show that, as the frequency of rotation increases, the oscillatory behaviour of flow field increases too. Generally, as can be observed in Figs 2.2 (a-e), the values and ranges of velocity in the x-direction are reduced as the angular velocity increases. This is attributed to the effects of ω on the initiation of the secondary flow or the y-component of the flow [27] . It should be noted that, the velocity is positive in the whole cross-section of channel when $\omega = 1$, whereas by increasing the ω, negative values are also observed in the velocity contour plots. This can be related to the fact that higher rotational centrifugal force pushes back the flow in x-direction. The reduction of the centre-line velocity, as shown in Figure 2f, confirms these observations. As can be seen, the velocity at the centre is reduced when the frequency of rotation increases becomes almost zero at $\omega = 20$. Furthermore, the position of maximum velocity moves from the centre of microchannel toward the walls when ω increases. The same trend was also reported by Chang and Wang [27] .

In Fig. 2.3, the transient 2-D dimensionless velocity $u(z,t)$ and the centre-line velocity profile are plotted for $\kappa = 5$ for the same range of angular velocity as

Fig. 2.2. As can be observed, the oscillatory behaviour of fluid flow didn't change by increasing the DH parameter. According to Eq. (2.17), the period of the velocity oscillations is equal to π/ω, regardless of the DH parameter. At higher rotational frequencies, a structure of boundary layer is observed. The boundary layer structure is found to be time dependent in the present work which was not noticed in earlier studies [27] and [90] .

However, It is clear that the velocity magnitude increased by increasing the DH parameter. At higher κ values the effect of induced electroosmotic forces (i.e., body force per unit volume on the fluid) becomes more influential, thus increasing the fluid velocity in x-direction. Also, the effect of ω on $u(z,t)$ is dampened at higher κ values. It becomes more evident when we compare the ratios of the maximum velocity represented on the range bars at different angular velocities. For example, $u_{\max}$ at $\omega = 1.0$ over $u_{\max}$ at $\omega = 2.5$ for $\kappa = 1$ and $\kappa = 5$ is 1.92 and 1.48, respectively. In order to examine the effect of large value for DH parameter on the x-component of the 2-D dimensionless velocity pattern and the centre-line velocity profile, κ was set at 1000 and the results are presented in Fig. 2.4. As shown, there is a small change in the range of the velocity with the change in ω. This is due to the significant effects of the electroosmotic forces at high κ values. The ratio of $u_{\max}$ at $\omega = 1.0$ over $u_{\max}$ at $\omega = 2.5$ in this case is about 1.0.

From Figs. 2.2-2.4 and Eq. (2.17) it can be concluded that the period of the velocity oscillations is constant (π/ω) and the rate of decay of oscillations is λ_n^2

which is independent of the DH parameter. The inertial oscillations are dissipated (i.e., third stage of development) through momentum diffusion.

The time interval is $0 < t < 3$. The velocity in the *y*-direction is also observed to follow an oscillatory behavior. However, the most important distinction between *u* and *v* is that for all positive values of ω and κ, the sign of the velocity in the y-direction is always negative. It means that the direction of the induced secondary flow is always –*y*.

The variations of *y*-component velocity and centre line velocities for $\kappa = 5$ and $\kappa = 1000$ were also investigated and the results are presented in Figs 2.6 and 2.7, respectively. The most important distinctions are as follow.

Higher rotation frequency leads to more oscillatory behaviour of flow velocity. Also, velocity gets some positive values when the DH parameter increases. This is directly linked to the effect of driving force of the electroosmotic forces at high κ values on the y-component of the velocity field. Furthermore, as the rotation frequency increases the probability of boundary layer initiation increases too which is in full agreement with previous reports [27] and [90] ..

Fig. 2.8 shows the evolutions of β over time ($0 < t < 3$) for $\kappa = 1000$ and different dimensionless angular velocities, ω = (a) 0.1, (b) 1.0, (c) π, (d) 5.0. It is indicated that the dimensionless angular velocity (ω) has a noticeable effect on the oscillatory behaviour of the flow. The smaller value of ω led to an almost non-oscillatory behaviour for $\beta(t)$ which was seen before for the velocity behaviour. As shown, the value of $\beta(t)$ increases significantly with the increasing

of ω. This means that, physically, the secondary induced flow enhances as the frequency of rotation increases. Also, the secondary induced flow parameter varies most rapidly for smaller value of ω which is in full agreement with the findings by Chang and Wang [27] .

In Fig. 2.9, the evolutions of β over time ($0 < t < 3$) for $\omega = 5$ and different DH parameter, κ = (a) 1.0, (b) 5.0, (c) 50, (d) 1000 is presented. It is clear that increasing the DH parameter (κ) leads to a decrease in the value of $\beta(t)$. For the large values of κ, $\beta(t)$ gradually approaches to 45. This means that for large κ, equal flows in both *x* and *y* directions are obtained which matches well with the Chang and Wang calculations to generate Fig. 2.8 in their study [27] . The governing equations are also solved numerically using MATHEMATICA. As can be seen in Figs. 2.8 and 2.9, the exact analytical solution results are in very good agreement with those obtained through numerical computation. Moreover, as indicated in Figs. 8 and 9, it should be pointed out that the effect of angular velocity gradually fades as the momentum diffusion increases which is also observed in Fig. (2.1). As a result, $\beta(t)$ approaches its steady state value, as reported by Chang and Wang [27] , when time is large enough.

2.5. Conclusions

In the present paper, the dynamics of rotationally induced secondary flow in an EOF between two parallel plates has been analytically studied. A general series solution expression for the non-dimensional velocity field and flow rate has been derived through the separation of variables technique. The effect of the Debye-Hückel parameter (κ) and the dimensionless angular velocity (ω) on the velocity

contour plots and parameter $\beta(t)$ has been examined. The main contribution of this study is providing a closed-form solution for the transient EOF in a rotating microchannel. It is found that the oscillatory behaviour of the fluid flow is only related to the ω while the DH parameter only changes the amplitude of the velocity field.

A time dependent structure of boundary layer was observed at higher rotational frequencies. The effects of ω on the initiation of the secondary flow was examined. Furthermore, the $\beta(t)$ parameter was investigated to show the effect of angular velocity and the Debye-Hückel parameter on the induced transient secondary flow in the y direction. It is found that when the Debye-Hückel parameter and the rotation parameter are high, $\beta(t)$ oscillates near 45 degree implying identical flow rates in x and y directions. Moreover, excellent agreement was found between the analytical results and the numerical results obtained by MATHEMATICA.

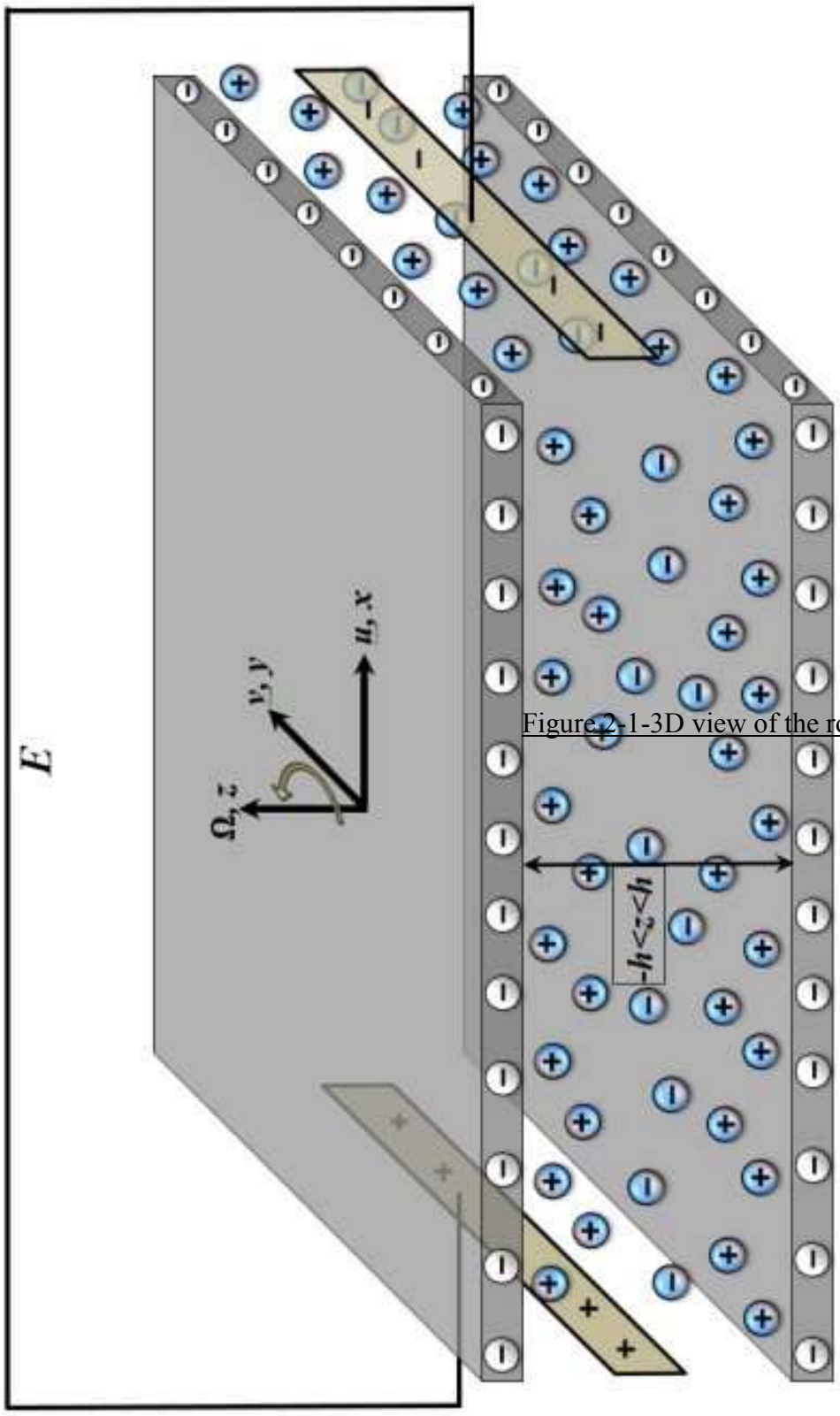

Figure 2-1-3D view of the rotating microchannel with EO

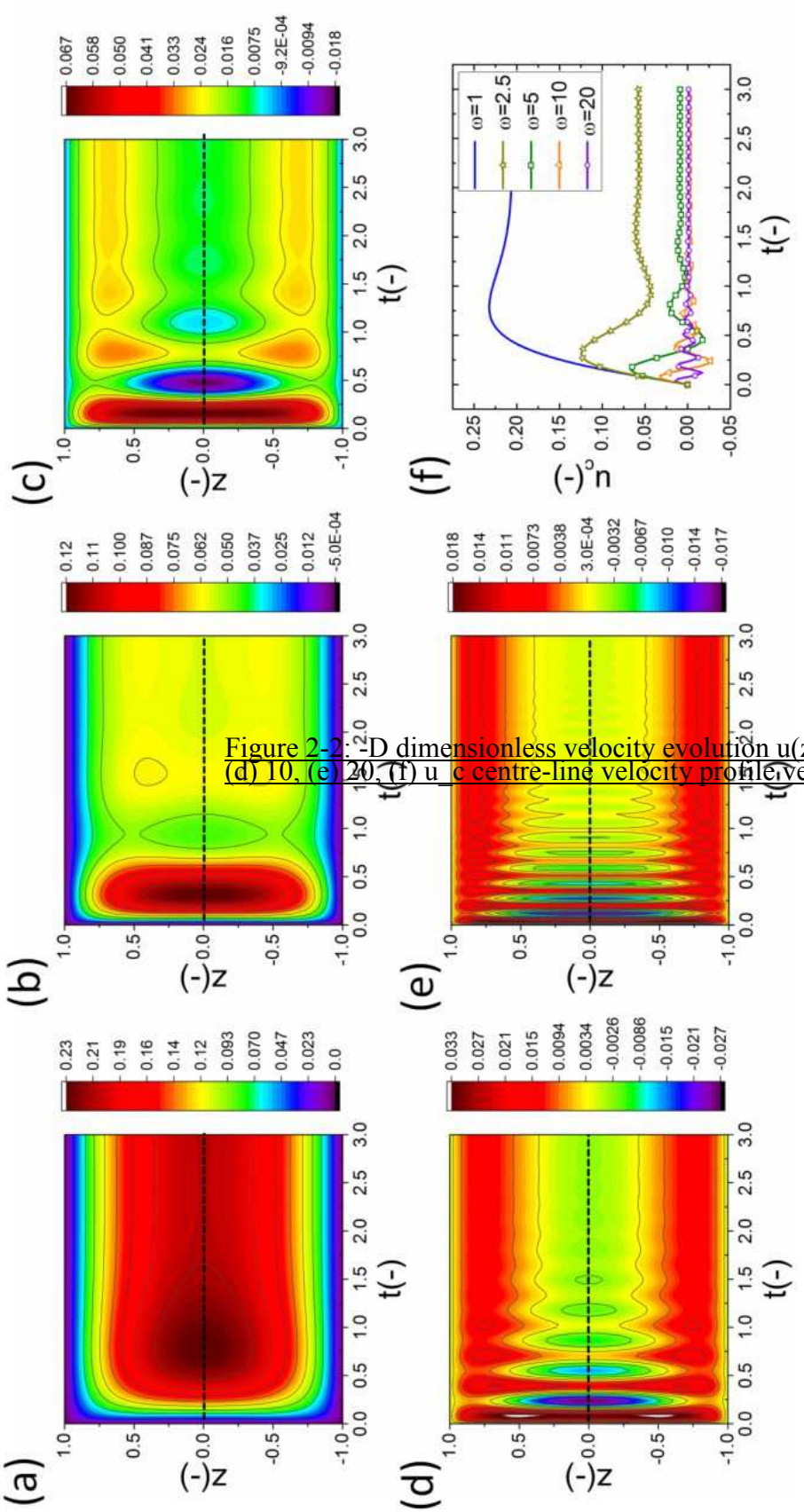

Figure 2-2: 2D dimensionless velocity evolution u(z,t) for κ=1. Dimensionless
(d) 10, (e) 20, (f) u_c centre-line velocity profile versus time.

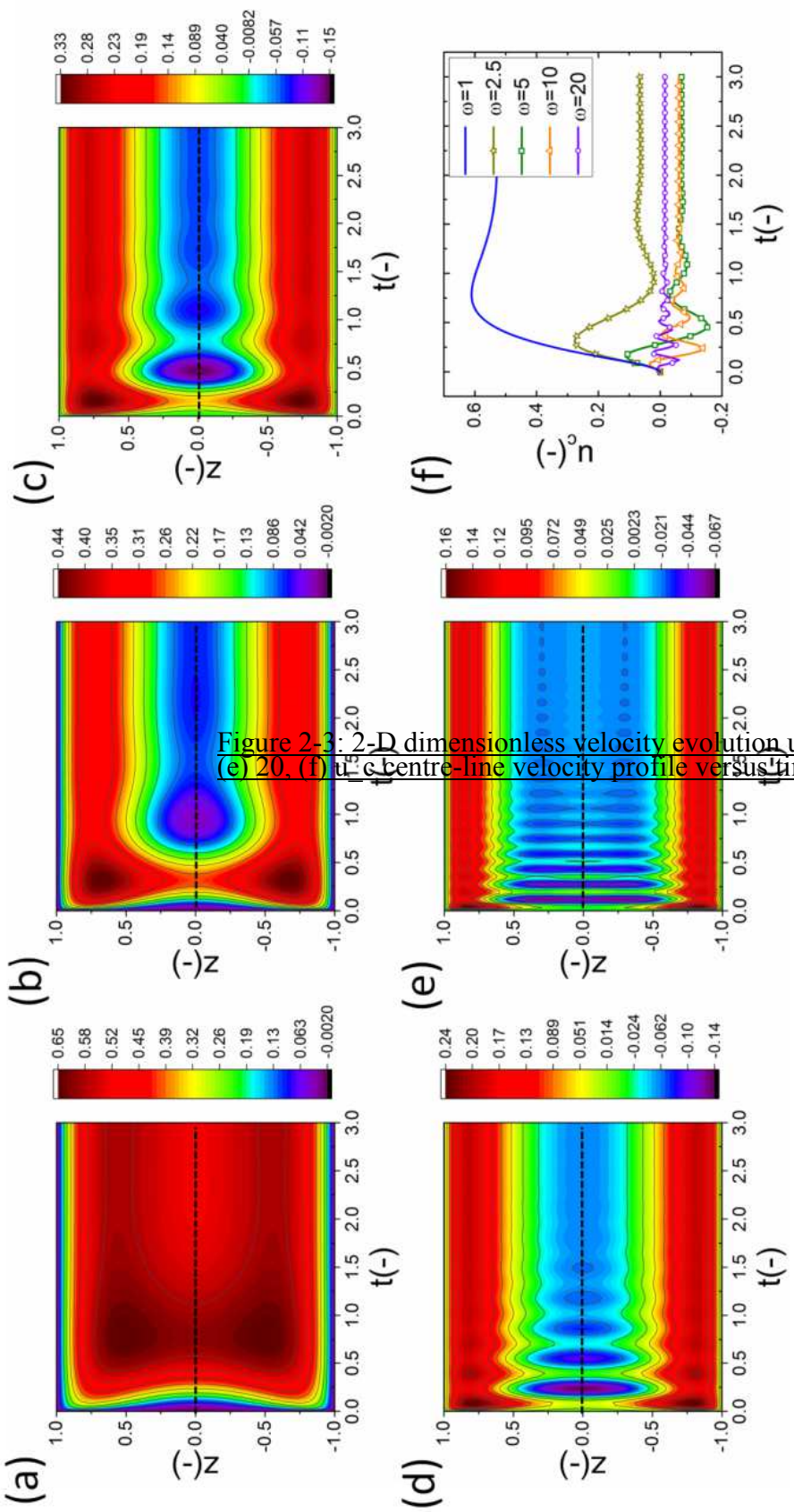

Figure 2-3: 2-D dimensionless velocity evolution u(z,t) for κ=5. Dimensionless (e) 20, (f) u* c centre-line velocity profile versus time.

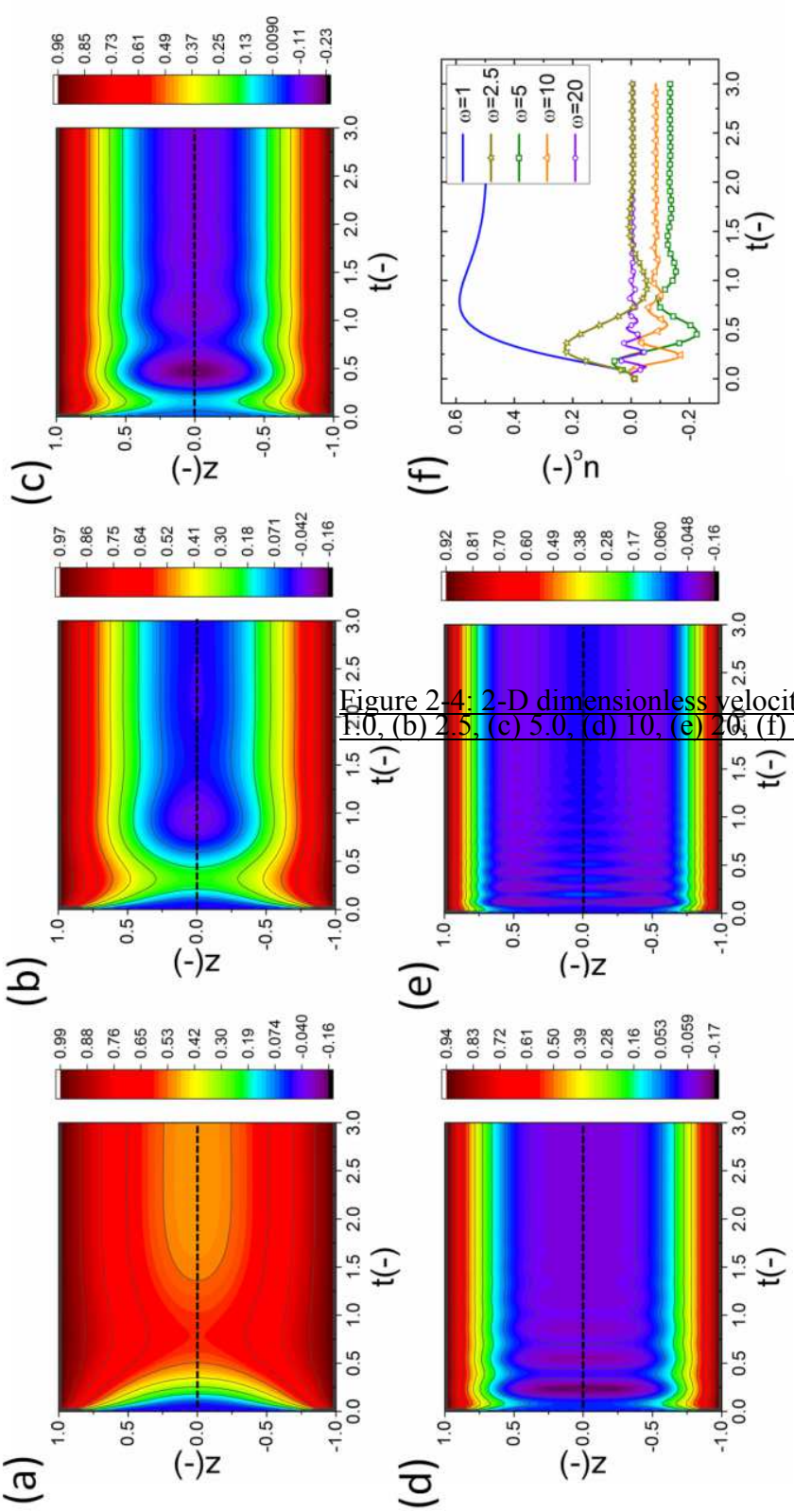

Figure 2-4: 2-D dimensionless velocity evolution u(z,t) for κ=1000. D
1.0, (b) 2.5, (c) 5.0, (d) 10, (e) 20, (f) u_c centre-line velocity profile v

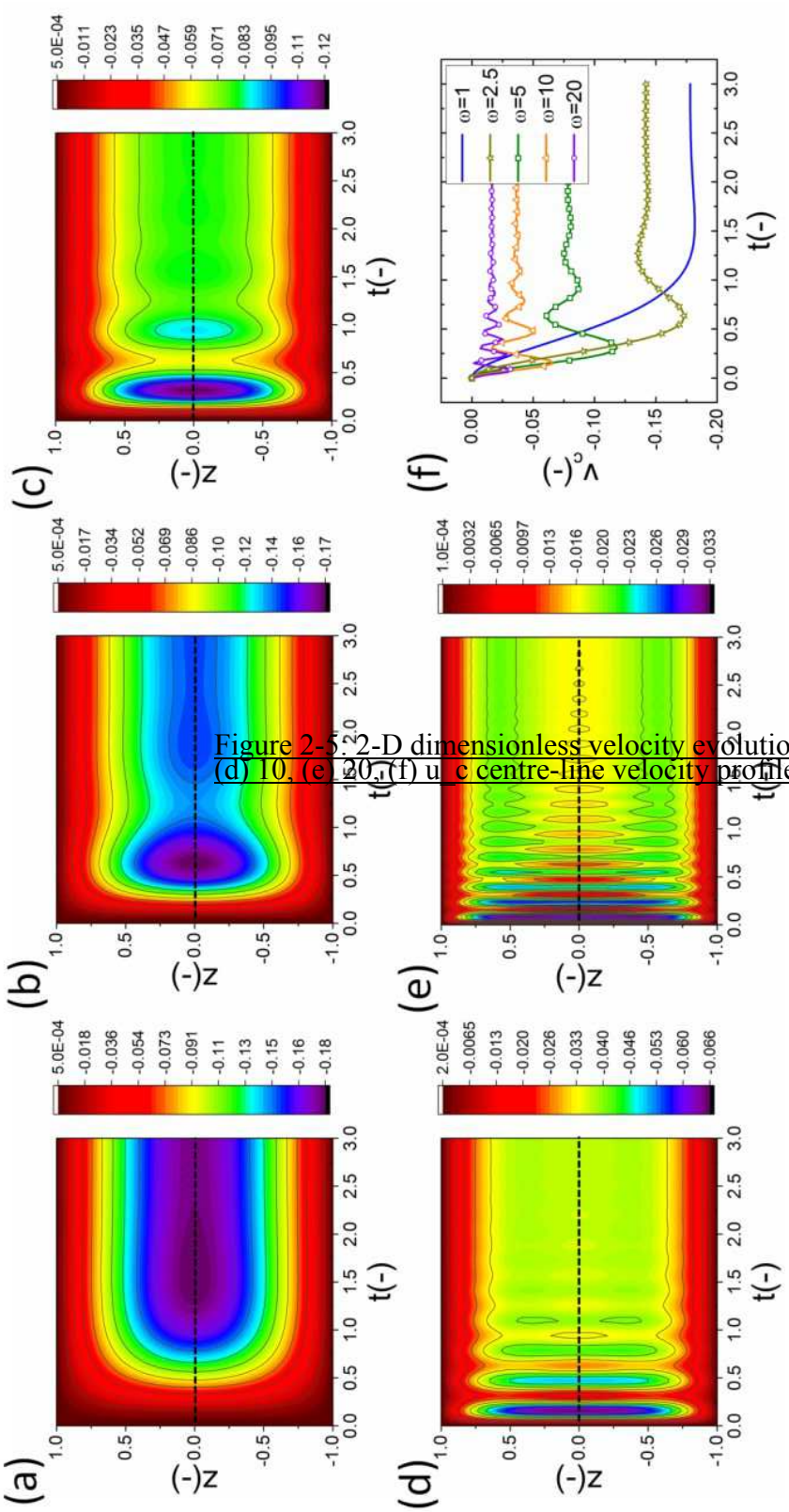

Figure 2-5: 2-D dimensionless velocity evolution u(z,t) for κ=1000. Dimensionl
(d) 10, (e) 20, (f) u_c centre-line velocity profile versus time.

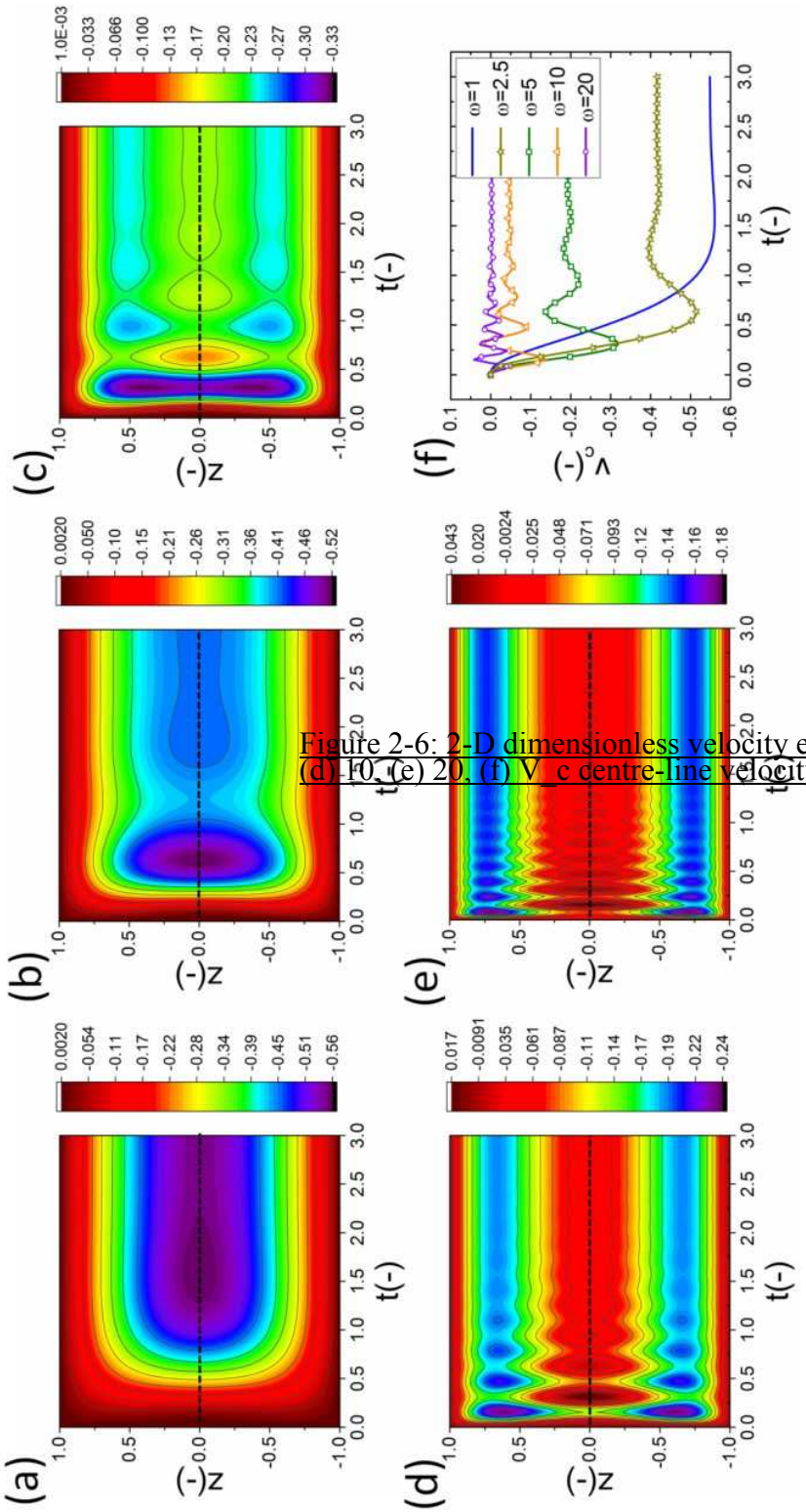

Figure 2-6: 2-D dimensionless velocity evolution v(z,t) for κ=5. Dimension
(d) 10, (e) 20, (f) V_c centre-line velocity profile versus time.

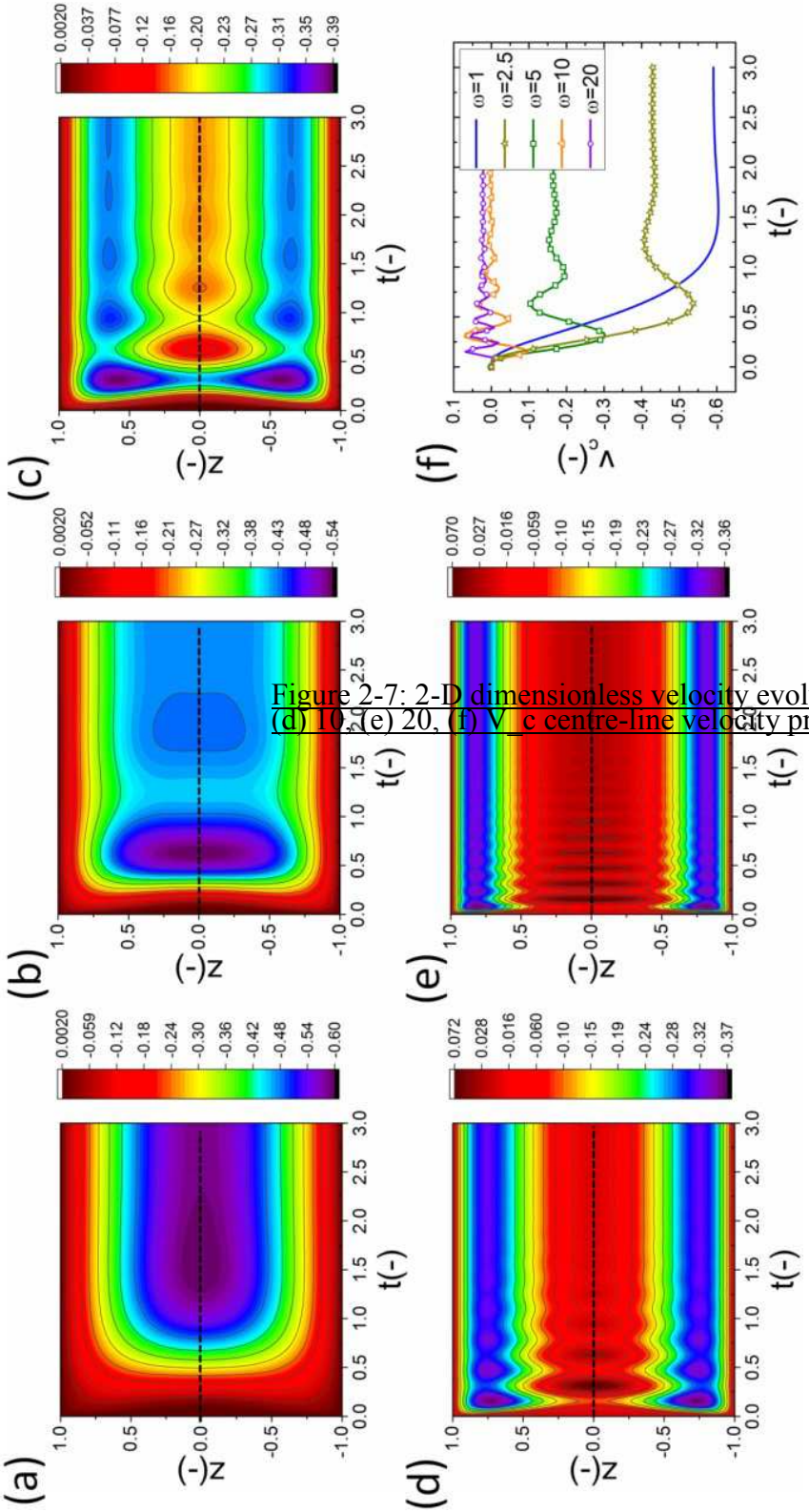

Figure 2-7: 2-D dimensionless velocity evolution v(z,t) for κ=1000. Dimension
(d) 10, (e) 20, (f) V_c centre-line velocity profile versus time.

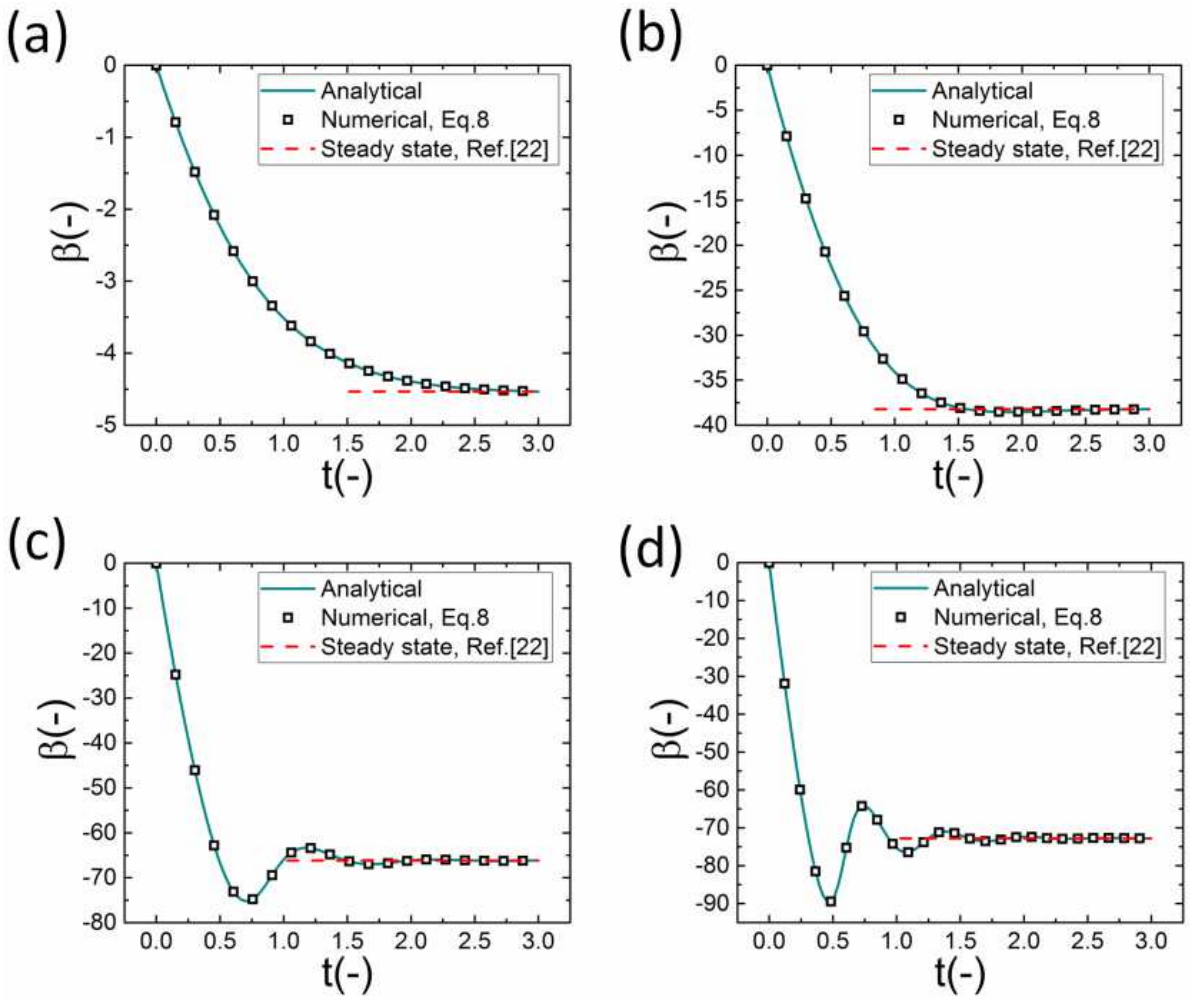

Figure 2-8: Evolutions of β with time for κ=1000. Dimensionless angular velocities, ω = (a) 0.1, (b) 1, (c) π, (d) 5.

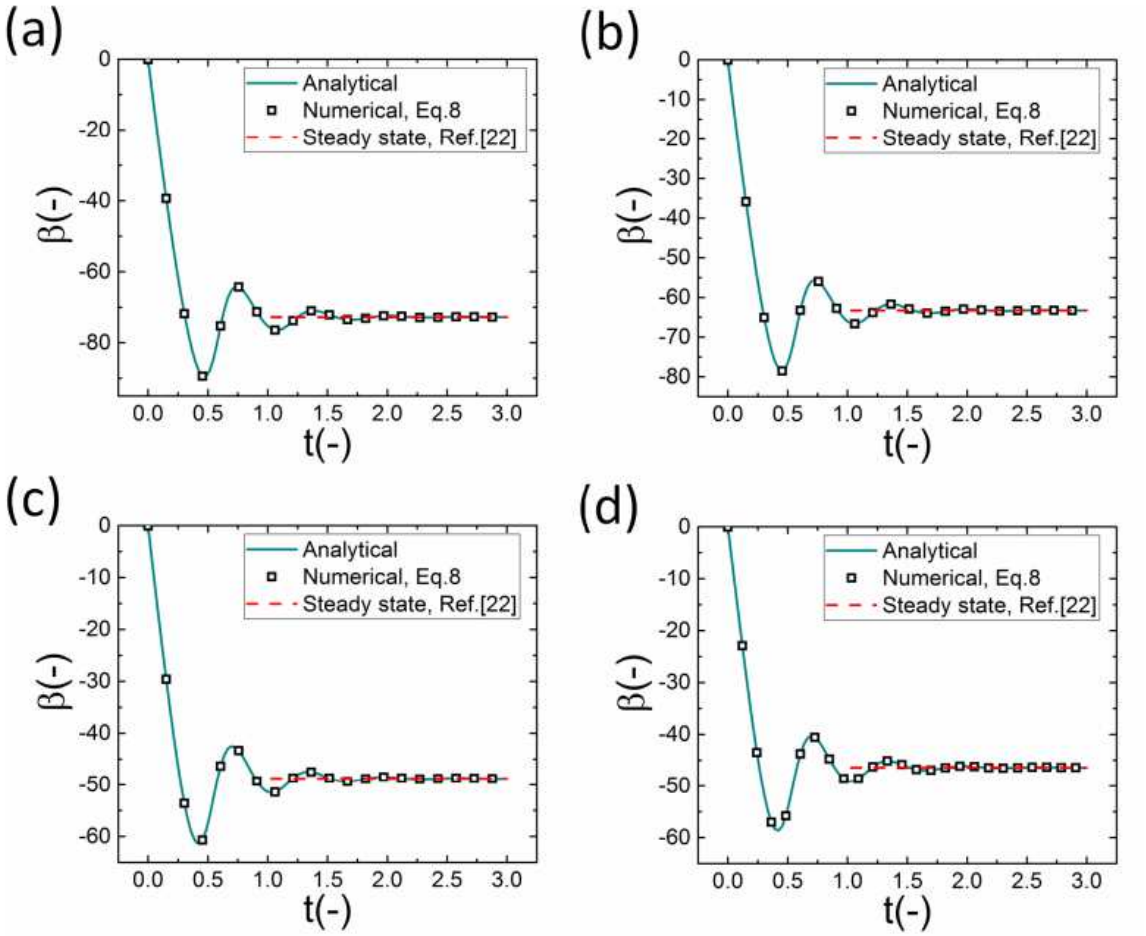

Figure 2-9: Evolutions of β with time for ω=5. κ = (a) 1.0, (b) 5.0, (c), 50, and (d) 1000.

CHAPTER 3: **Effect of intrinsic angular momentum in the capillary filling dynamics of viscous fluids**

3.1. Introduction

In recent years, there has been a significant interest in research works related to the fluid flow through microchannels as a result of unbalanced capillary forces. In the pioneering studies led by Lucas [52] and Washburn [53] , the mechanical balance between the capillary, viscous and gravitational forces is applied to describe the dynamic process involved in capillary rise for laminar flows. The well-known Lucas-Washburn (LW) [52] and [53] equation provides a proportionality [71] inertial term and defining a finite initial velocity, called Bosanquet velocity. However, using high resolution experiments, Kornev and Neimark [95] found discrepancies between experimental velocities and those obtained from Bosanquet equation. So far various theoretical and numerical studies have been conducted on the dynamic filling of capillaries. Srivastava and Burns[74] [96] developed a quick and accurate viscosity measurement based on capillary pressure-driven flow of non-Newtonian fluids inside microfluidic channels. In a numerical/experimental study, Lavi *et al*.[75] [97] showed that disregarding the effects of the inertia and the dynamic contact angle (i.e., the assumption made in the LW equation) causes inaccurate results in assessment of the capillary radius and the equilibrium contact angle. Mondal *et al*.[76] [98] investigated the effects of patterned wettability gradient and an external electric field on contact-line dynamics of two immiscible fluids. They showed that the stick-slip motion velocity of contact line (the rate of combined deformation

behavior of semi-macroscopic contact region) is a strong function of the interfacial electrokinetics. Tas *et al*.[77] [60] and Persson *et al*. [99] reported a smaller rate of filling of glass nanochannels by de-ionized water compared to an uncharged capillary condition , which might be attributed to the retarding electrical effect of capillary wall.

In all above studies, since there is no spin angular momentum in flow of point-like particles, the intrinsic angular momentum (or spin) and it's coupling to the translational momentum are not considered in derivation of the Navier-Stokes (NS) equation [100] . In macroscopic systems, this coupling is not taken into account due to small effects of fluid molecular behaviors [101] , whereas at small length scales, molecular fluids behaves differently as it is significantly affected by the coupling between the molecular spin angular velocity and the fluid streaming velocity [102] . In the molecular fluids, non-central forces result in non-symmetric pressure tensor, thereby forming additional coefficients of viscosity [73] which are the main reasons for the rotation-translation coupling [24] .

Dahler and Scriven [72] derived the governing equations describing the dynamics of the molecular fluids considering the spin velocity of the particles. This angular velocity is not necessarily one-half the vorticity or the rotation rate of the fluid. This difference was captured by introducing a physical parameter known as vortex viscosity which is shown to be a tensor quantity [73] and [74] . In fact, the vortex viscosity quantifies the antisymmetric portion of the stress and can be properly estimated for a dilute suspension [75] . Condiff and Dahler [76] assigned continues spin field to the rotation of the molecular subunits. The

interaction of internal spin is then described by antisymmetric stress and generalized NS equations for the velocity and spin fields. They applied a body-torque density to describe the interaction of polar fluid with electric field as well as the vortex viscosity.

The concept of coupling rotational and translational motions of molecules can be utilized for pumping applications. Zaitsev and Shliomis [77] used vortex viscosity coefficient to examine the behavior of ferromagnetic suspension in a uniform rotating magnetic field where each suspended particle had its own intrinsic magnetic moments. The particles start rotating due to the rotation of the field which generates the macroscopic motion (pumping) of the medium. They also calculated the power and the friction torque acting on the walls of a cylinder cavity filled with ferromagnetic suspension. Joseph and Aluru [103] used a molecular dynamics (MD) simulation to attain a net water molecule transport due to a coupling between rotational and translational motions of molecules. Bonthuis *et al.* [104] also used MD simulation to investigate the flow generation in water-filled nanochannels. For this purpose, they applied the generalized NS equations including the molecular angular momentum along with appropriate boundary conditions. It was shown that, in the case of planar geometry, the static electric fields do not induce fluid flow, while hydraulic power is generated when the electric fields rotate. Besides, Hansen *et al*. [71] used non-equilibrium molecular dynamics (NEMD) simulations to quantitatively demonstrate the necessity of intrinsic angular momentum in the fluid-mechanical description of nanoflows of molecular liquids. Comparing results of the streaming velocity profiles, they have

shown that the classical NS theory without the coupling phenomenon cannot predict the velocity profile correctly. Felderhof [105] considered the extended NS equation to analytically study the pumping hydrodynamic of ferrofluids with rotating suspended particles through a planar duct/circular tube by means of an electric wave.

The extended NS equations of fluids with rotating suspended particles are affected by spin viscosity as well as vortex viscosity. Unlike vortex viscosity, the evaluation of the spin viscosity is not well established [106] . A few studies in literature have been conducted to evaluate the effect of spin viscosity on the behavior of the molecular fluids. Zaitsev and Shliomis [77] showed that, for ferrofluids involving the internal angular momentum, the spin viscosity depends upon the viscosity of the fluid. Different ranges for spin viscosity are proposed in the literature [108] and [109] . They estimated values based on comparison of flow measurements and the theoretical results of the extrapolated wall velocity from the regular perturbation method. The reported values lie in the range of 10^{-8} and 10^{-12} kg.m/s. Felderhof [74] obtained a large value of spin viscosity by conducting an analytical study on the fluid flow in spherical geometry for a uniform rotating magnetic field.

To the best of our knowledge, no study has been conducted to date to explore the effect of angular momentum on the capillary filling dynamics of fluids. In the present work, the effect of spinning particles on the capillary filling dynamics has been investigated. It is shown that spinning particles couple rotational and translational movements. Three different time stages during the capillary filling and their dependence on the spin viscosity and vortex viscosity are thoroughly examined. The results for capillary filling without rotating particles (as a limiting case) are compared with literature data.

3.2. Mathematical Formulation

The geometry for the present analysis is an open ended capillary filled by so called incompressible molecular fluid containing spinning particles (Fig. 1). The capillary consists of two parallel plates kept at $y = -h$ and $y = h$ at Cartesian coordinate system.

Before proceeding to examine the specific case of molecular fluid, a viscous fluid filling the capillary is considered as a base case. First, the equations describing capillary filling are derived by considering the liquid inertia. An average position x_f is considered as the filling length or the capillary front at time t. Following Newton's second law of motion, the equation of motion for the capillary advancement can be obtained from the force balance per unit width on the liquid column [110] :

$$\frac{d}{dt}\left(2h\rho x_f \frac{dx_f}{dt}\right) = F_{\mathrm{st}} + F_{\mathrm{visc}} + F_0, \tag{3-1}$$

where F_{st} is the force due to the surface tension, F_{visc} is the viscous resistance at the walls to the motion of the capillary front, F_0 is the force field and ρ is the density of the fluid.

The surface tension force can be expressed as $F_{\mathrm{st}} = 2\gamma_{\mathrm{s}}\cos(\theta)$. Here, γ_{s} is liquid-vapor surface tension coefficient and assumed to be constant. Also, θ is the constant equilibrium contact angle at the fluid-solid-gas interface. The total viscous force can be expressed as $F_{\mathrm{visc}} = 2\tau_{xy}x_f$ with τ_{xy} being the viscous stress on the walls of microchannel.

In channels filled with molecular fluid including spinning particles, the rotational degree of freedom of constitutive particles in the filling fluid or suspension is considered. The fluid may also be subjected to a local force density $\boldsymbol{F}$ and a torque density $\boldsymbol{N}$. These effects are taken into account in the equations of motion or the extended NS equations [76] . Hence, the equations of motion for momentum and spin are written as follow:

$$\rho\boldsymbol{v}.\nabla\boldsymbol{v} = \eta\nabla^2\boldsymbol{v} - \nabla p - \zeta\nabla\times(\nabla\times\boldsymbol{v} - 2\boldsymbol{\omega}) + \boldsymbol{F}, \tag{3-2.a}$$

$$\rho I\boldsymbol{v}.\nabla\boldsymbol{\omega} = \eta'\nabla^2\boldsymbol{\omega} + \mathbf{2}\zeta(\nabla\times\boldsymbol{v} - 2\boldsymbol{\omega}) + \boldsymbol{N}, \tag{3-2.b}$$

where $\boldsymbol{v}$ is the flow velocity vector, η is the shear viscosity, p is the pressure, ζ is the vortex viscosity, $\boldsymbol{\omega}$ is the particle spinning rate, η' is the spin viscosity, and I is the moment of inertia per unit mass. The flow velocity and the particle spin rate satisfy $\nabla.\boldsymbol{v} = 0$ and $\nabla.\boldsymbol{\omega} = 0$.

The presence of non-central forces in the hydrodynamic of molecular liquids gives rise to an antisymmetric stress tensor that leads to the formation of the vortex or rotational viscosity [73] . The effect of vortex viscosity is shown as the

third term on the right hand side of Eq. (3-2.a). The effect of spin viscosity is originated from the rotation of individual molecules in molecular fluid around their individual mass centres. This effect is captured in the first term on the right hand side of Eq. (2.b) [112] .

In this study pressure is considered constant and the force and the torque densities are assumed as following:

$$\boldsymbol{N} = \boldsymbol{0}, \quad \boldsymbol{F} = (0,0,F_0), \tag{3-3}$$

where F_0 is a constant force. Velocity and spin rate vectors are also assumed to have z and y components ($v_z(x)$ and $\omega_y(x)$, respectively) as following:

$$\boldsymbol{v} = \big(0,0,v_z(x)\big), \quad \boldsymbol{\omega} = \big(0,\omega_y(x),0\big), \tag{3-4}$$

With the above mentioned assumptions, the governing equations (2) can be simplified as (see Appendix):

$$(\eta+\zeta)\frac{d^2v_z}{dx^2} + 2\zeta\frac{d\omega_y}{dx} + F_0 = 0, \tag{3-5}$$

$$\eta'\frac{d^2\omega_y}{dx^2} - 2\zeta\left(\frac{dv_z}{dx} + 2\omega_y\right) = 0.$$

It is clear that if we set $\eta' = 0$ then Eq. (3-5) yields the simple Poiseuille flow. Here, the no slip boundary condition is applied for velocity and spin rate at the wall of the channel. Having developed the governing NS equation, capillary filling dynamics associated with this equation needs to be investigated.

In order to examine the effect of uniform force density, a condition with vanishing torque and constant force is considered. Therefore, the non-dimensionalized form of the flow velocity is written as follows [105] :

$$v_z = v_{\text{ref}}\Big[1 - (\tfrac{y}{h})^2 + A(\cosh(\kappa y/h) - \cosh(\kappa))\Big], \tag{3-6}$$

where $v_{\text{ref}} = \frac{F_0 h^2}{2\eta}$, $A = \frac{1}{2\eta h}\frac{\kappa\eta'}{\sinh(\kappa h)}$ and $\kappa = \sqrt{4\eta\zeta/\eta'\eta_e}$ $(\eta_e = \eta + \zeta)$

Using expression (3-6) for the velocity field, the average velocity can be found as:

$$v_{\text{avg}} = 2v_{\text{ref}}\left[\frac{2}{3}h + A\left(\frac{\sinh(h\kappa)}{\kappa} - h\cosh(\kappa)\right)\right], \tag{3-7}$$

where $v_{\text{avg}} = 2\int_0^h v_z dy$. Combining Eqs. (3-6) and (3-7) and replacing v_{avg} with $\frac{dx_f}{dt}$, the velocity can be evaluated in terms of the average velocity and the liquid front velocity (i.e., $\frac{dx_f}{dt}$) as:

$$v = \frac{1}{2A_1}\frac{dx_f}{dt}\left[1 - (\frac{y}{h})^2 + A(\cosh(\kappa y/h) - \cosh(\kappa))\right]. \tag{3-8}$$

where $A_1 = \frac{2}{3}h + A\left(\frac{\sinh(h\kappa)}{\kappa} - h\cosh(\kappa)\right)$. The total viscous resistance to the flow is found to be

$$F_{visc} = 2x_f\tau_w \text{ at } y = -h, \tag{3-9}$$

where $\tau_w = (\eta + \zeta)\frac{\partial v}{\partial \bar{y}}$ is the shear stress at walls. Therefore, using Eqs. (3-7) and (3-9), the viscous force can be written as follows:

$$F_{\text{visc}} = \frac{2hx_f(\eta+\zeta)}{A_1}\frac{dx_f}{dt}\left[-\frac{2}{h} + A\kappa\sinh(\kappa h)\right], \tag{3-10}$$

Finally, by substituting Eq. (3-10) into the force balance equation (Eq.3-1), the equation governing the capillary dynamics is derived:

$$\frac{d}{dt}\left(2\rho h x_f\frac{dx_f}{dt}\right) = 2\gamma_s\cos(\theta) + \frac{2hx(\eta+\zeta)}{A_1}\frac{dx}{dt}\left[-\frac{2}{h} + A\kappa\sinh(\kappa h)\right], \tag{3-11}$$

In order to simplify the analysis procedure, it is common to define dimensionless variables. Therefore, for non-dimensionalizing equation (3-11), the dimensionless variables are defined as follows:

$$\overline{x_f} = \frac{x_f}{h}, \bar{t} = \frac{t}{t_{\mathrm{ref}}}, \tag{3-12}$$

where $t_{\mathrm{ref}} = \sqrt{\rho h^3/\gamma_{\mathrm{s}}}$.

Substituting the dimensionless variables (3-12) into Eq. (3-11) and dropping the asterisks the following dimensionless governing equation is obtained for the capillary filling dynamics:

$$\frac{d}{dt}\left(x_f \frac{dx_f}{dt}\right) = C - Dx_f \frac{dx_f}{dt}, \tag{3-13}$$

where $C = \frac{\gamma_{\mathrm{s}} t_{\mathrm{ref}}^2}{\rho h^3}\cos(\theta)$ and $D = \frac{\eta t_{\mathrm{ref}}[-2+Ah\kappa\sinh(\kappa h)]}{\rho h A_1}$.

Featuring the inertial and viscous terms, one can find the solution of Eq. (3-13) by integrating it twice with zero boundary condition as [110] :

$$x_f(t) = \sqrt{\frac{2C}{D}\left(t - \frac{1-e^{-Dt}}{D}\right)}. \tag{3-14}$$

In the next section, different regimes for the capillary filling dynamics will be discussed.

3.3. Scaling estimates

To demonstrate the significance of viscosity coefficients, scaling analysis must be applied to understand different regimes in the capillary filling problem. The ratio of the resisting viscous forces and the driving capillary forces is examined thorough scaling estimate process. As mentioned earlier, the following scaling: $F_{\mathrm{st}} \sim \gamma_{\mathrm{s}} h$ and $F_{\mathrm{visc}} \sim (\eta + \zeta)\left(\frac{\partial v}{\partial y}\right) x_f h \sim (\eta + \zeta) v_0 x$ with $v_0 \sim \frac{x_f}{t}$ are considered. Using the scaling, it can be easily found that $\frac{F_{\mathrm{visc}}}{F_{\mathrm{st}}} \sim h{x_f}^2/\gamma_{\mathrm{s}} h t$. To scale time, the fluid transport is assumed to occur merely because of capillary

force so F_{st} can be obtained by $mdv/dt \sim F_{\mathrm{st}}$, and thus $t \sim x_f\sqrt{\rho h/\gamma_{\mathrm{s}}}$. Hence, the ratio of forces can be written as follows [62] :

$$\frac{F_{\mathrm{visc}}}{F_{\mathrm{st}}} \sim \frac{\eta x_f}{\gamma_{\mathrm{s}} h}\sqrt{\frac{\gamma_{\mathrm{s}}}{\rho h}} \sim \frac{(\eta+\zeta)}{\sqrt{\rho\gamma_{\mathrm{s}} h}}\left(\frac{x_f}{h}\right) = \mathrm{Oh}\left(\frac{x_f}{h}\right), \tag{3-15}$$

where Oh is the modified Ohnesorge number. In the following three distinct regimes encountered in capillary filling of viscous fluid with spinning particles are defined:

(1) For $\mathrm{Oh}(x_f/h) \ll 1$, the influence of the viscosity is negligible in comparison to the capillary forces and the capillary filling dynamics of the fluid is purely dominated by inertial forces. In this region, the balance between the inertial and the capillary forces (i.e., $\gamma_{\mathrm{s}} h \sim \frac{d}{dt}\left(\rho x_f h^2 v\right)$ is the main reason for the capillary filling. Using time and velocity scaling, the linear scaling law can be obtained between time and front position as $x_f \sim t\sqrt{\gamma_{\mathrm{s}}/\rho h}$. This can also be acquired from Eq. (3-14) for small time parameter as $x(t) = \sqrt{C}t$. it can be defined that $t \ll \tau_c = \sqrt{\rho h^3/\gamma_{\mathrm{s}}}$. Similar to the condition $\mathrm{Oh}(x/h) \ll 1$, the time $t \sim \tau_c$ is used to represent the inviscid regime [66] .

(2) For $\mathrm{Oh}(x_f/h) \sim 1$, the capillary flow is driven by the balance of the viscous and the capillary forces ($F_{\mathrm{visc}} \sim F_{\mathrm{st}}$). This regime, called Intermediate or visco-inertial stage, is exactly shown by Eq. (3-14). It can be easily obtained that in the visco-inertial stage $t = \tau_{vi} = \rho h^2/(\eta + \zeta)$.

(3) For $\mathrm{Oh}(x_f/h) \gg 1$, the viscous effects overwhelm the capillary forces and the flow becomes purely viscous. Lucas [52] and Washburn [53] also neglected the influence of inertia in this last regime where the time parameters are

sufficiently large. At this regime, one may find the capillary front non-dimensional position as $x_f(t) = \sqrt{2Ct/D}$. A time scale for this regime can be defined above which only viscous effects exist. This regime is defined as $t \gg \tau_{vi} = \rho h^2/(\eta + \zeta)$.

3.4. Numerical results and discussions

In this section, the developed analytical solution is used to obtain the capillary filling characteristics of a fluid under the effect of spinning particles. Results are presented for two different channel heights $2h = 200 \text{ and } 400$ μm. Shear viscosity(η) and density (ρ) are 0.001 kg/ms and 1000 kg/m^3, respectively.

First the effect of spin and vortex viscosities on the viscous force, as the main force influencing the capillary filling dynamics, is investigated. In Figs. 3-2(a and c), the non-dimensional viscous force is plotted against time parameter for different spin viscosity of $\eta' = 10^{-10}$, 10^{-11}, 10^{-12} kg/ms, constant vortex viscosity of $\zeta = 5 \times 10^{-4}$ kg/ms and two different channel heights of 200 and 400 μm. Viscous force is non-dimensionalized with respect to its maximum value at steady state. It can be seen that the viscous force increases over time and reaches to its steady state limiting value for all cases. As the spin viscosity increases, the time required to achieve the maximum force decreases. At a given time, when η' decreases the viscous force declines, thereby facilitating the movement of the capillary front. In addition, as the channel height increases, the time required to reach the maximum viscous force decreases which is in agreement with literature [110] .

Figs. 3-2(b and d) show the effect of vortex viscosity($\zeta = 0.001, 0.0005, 0.0001$ kg/ms) on the viscous force at constant shear viscosity of $\eta' = 10^{-11}$ kg/ms and two different channel heights of 200 and 400 μm. Similar transient trend as that observed for the effect of spin viscosity on the viscous force is also noticed for vortex viscosity. Increasing the vortex viscosity also enhanced the viscous force. This means that the viscous forces become stronger at higher vortex viscosities that impede the movement of the capillary front.

Fig. 3-3 shows the non-dimensional capillary penetration distance(x) as a function of non-dimensional time (t) for different spin viscosity parameter ($\eta' = 10^{-10}, 10^{-11}$ and 10^{-12}kg/ms), vortex viscosity ($\zeta = 0.001,\ 0.0005,\ 0.0001$ kg/ms) and channel heights of $2h = 200$ and 400 μm. Results show that the penetration distance decreases as spin and vortex viscosities increases for both channels. It is observed that as the spin and vortex viscosities increase the front position reduces which can be attributed to the enhancement of viscous force by increasing both viscosities as presented in Fig. 3-2. This behavior was also observed for the channel flow where the fluid flow velocity increased when spin viscosity decreased [75] . Moreover, as the viscosities increase the front position results deviate more significantly from the no-angular-momentum (NAM) case. Increasing the channel height from 200 μm to 400 μm clearly increased the penetration depth. This might be attributed to the fact that as the height increases the viscous force decreases (see Eq (10)) and subsequently, the penetration depth increases. According to Figure 3-3 (a-d), as the height of the channel decreases

the front position trend deviates more from the linear behavior which is in agreement with results obtained by Bandopadhyay *et.al*. [110] .

In order to identify the existence of different regimes, the variation of front position is plotted in log-scale for the case of $\zeta = 5 \times 10^{-4}$ kg/ms and $2h = 200\ \mu$m in Fig. 3-3(e). According to this figure, there are three different time stages during the capillary filling which are found using the Quere [56] and Lucas-Washburn [53] limiting case solutions: (i) inertia force dominated, (ii) visco-inertial stage, and (iii) viscous dominated regions. The applied scaling law in the present work is validated for the linear regime with the results provided by Quere [56] . In the first regime (i.e., the linear stage) the capillary filling is independent of the fluid viscosities. At longer times however, the viscosities start affecting the penetration distance in the intermediate or visco-inertial regime and the capillary flow is driven by the balance of the viscous and the capillary forces.

In the second regime, x is substantially large so that it can be assumed that $\mathrm{Oh}(x/h) \sim 1$ [62] . In the last regime, the behavior of front position is mostly affected by spin viscosity. As can be seen the results in this region are comparable to Lucas-Washburn results [52] and [53] in which the influence of inertia is neglected. Here, x has become so large that $\mathrm{Oh}(x/h) \gg 1$ and the limiting trend for front position is $x(t) = \sqrt{2Ct/D}$. Taking a closer look at Fig. 3-3(e) shows that as spin viscosity increases the time required for the front position to reach the limiting value increases which matches well with the results presented in Fig. 3-2(a). Furthermore, as observed in Fig. 3-2, the viscous force became steady after

about *t*=1000. This affects the front end variations and leads to generation of purely viscous regime after *t*=1000 where viscous force is constant.

As shown in the scaling section, the linear regime can be characterized with $t \ll \tau_c = \sqrt{\rho h^3/\gamma_s}$. For example, for $h = 100$ and $200\ \mu$m, it can be obtained that $\frac{\tau_c}{t_{\text{ref}}} = 1$. This shows that for $t \ll t_{\text{ref}}$ a perfect linear relationship between the front position and the time parameter must exist. For the intermediate regime, based on the balance between both viscous and inertial forces the time around which this regime happens is obtained as $t = \tau_{vi} = \rho h^2/(\eta + \zeta)$. For $h = 100$ and $200\ \mu$m $t = 77.1$ and $t = 109.1$, respectively. This shows that as the thickness of the channel increases the time required to reach the intermediate regime increases. A time beyond which the behaviour of fluid front position is affected only by viscosities of the fluid can be estimated by. This time is obtained to be τ_{vi}. It means that for times after τ_{vi} $(t \gg \tau_{vi})$ the capillary flow regime becomes viscous dominated.

3.5. Conclusion

An analytical model is presented to describe the dynamics of capillary filling. The filling viscous fluid contains spinning particles which contributes to spin and vortex viscosity. The results show that when viscosities (spin and vortex viscosity) increase the behavior of front position no longer varies linearly with time. Also, an increase in both spin and vortex viscosity leads to a decrease in the front position of the moving liquid. Three distinct regimes have also been demonstrated for the capillary filling behavior. In the first regime the effects of

viscosities were not dominant. In the intermediate or visco-inertial region, the balance of the viscous and the capillary forces drives the capillary flow. Hence, effect of using molecular fluid on capillary filling dynamics is more evident in the intermediate region. Lastly, the behavior of front position is mostly affected by spin viscosity in the third viscous-dominated region. It is observed that as spin and vortex viscosities increase the viscous force enhance and consequently the penetration rate declines. It is shown that the effect of vortex viscosity mainly appears in the viscous force and it does not affect the capillary dynamics at the inertial stage. The data provided in this study are also compared to some limiting cases provided in literature and excellent agreement is observed.

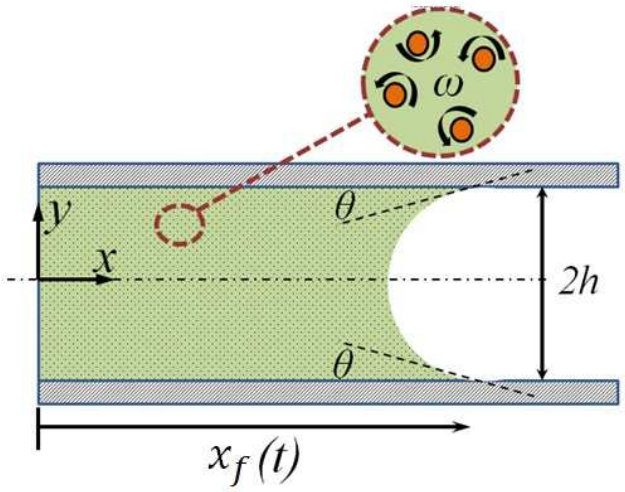

Figure 3-1 Schematic of capillary filled with spinning particle.

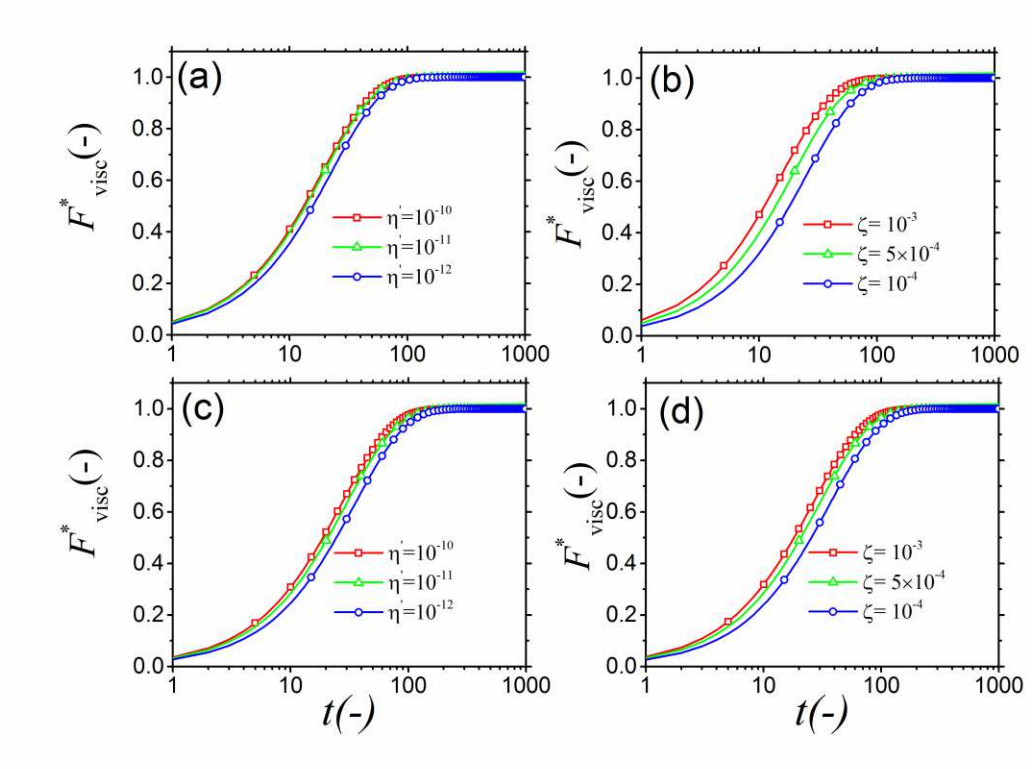

Figure 3-2 Variation of viscous force over time: effect of spin viscosity at constant $\zeta = 5 \times 10^{-4}$ kg/ms and and vortex viscosity at constant $\eta' = 10^{-11}$ kg/ms and (a,b for $2h = 200$ μm and c,d for $2h = 400$ μm).

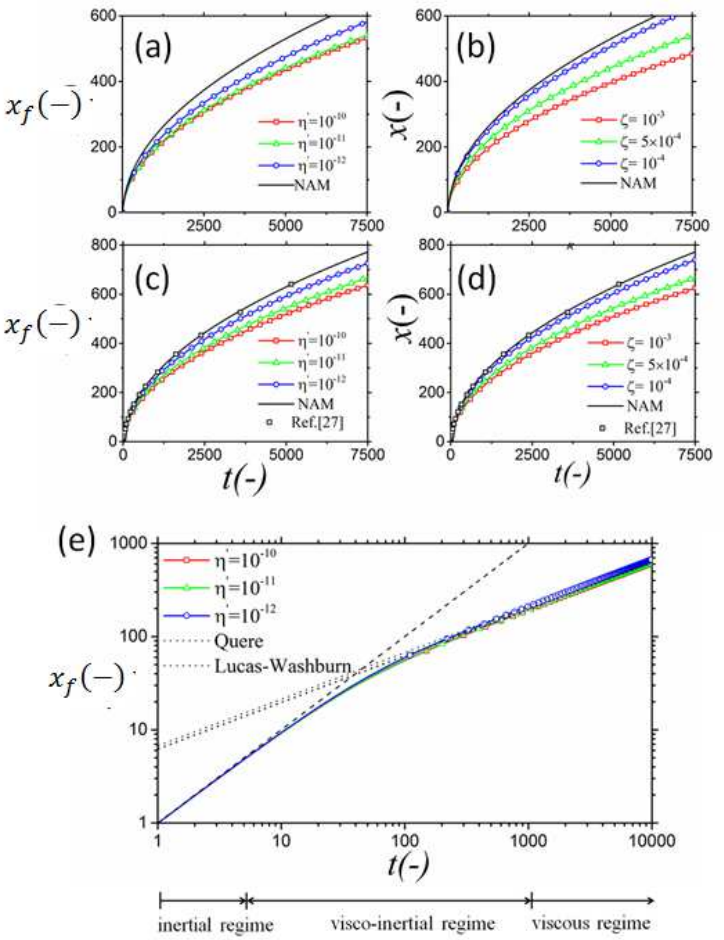

Figure 3-3 Non-dimensional penetration depth, $x_f(-)$ versus non-dimensional time $t(-)$: effect of spin and vortex viscosity. Channel height (a,b) $2h = 200\ \mu$m, (c,d) $2h = 400\ \mu$m (e) effect of spin viscosity in log-log scale for $\zeta = 5 \times 10^{-4}$ kg/ms and $2h = 200\ \mu$m.

CHAPTER 4: **Conclusions and Future Directions**

4.1. Summary and Conclusions

In this research, an analytical investigation is done on the dynamics of rotationally induced secondary flow in an EOF between two parallel plates. The separation of variable method is used to obtain a general series solution expression for the non-dimensional velocity field and flow rate. A closed-form solution for the transient EOF in a rotating microchannel is obtained which has not been reported before. Effects of different parameters on the behaviour of the fluid flow have been examined. The Debye-Hückel parameter (κ) and the dimensionless angular velocity (ω) are found as the most important parameters in this analysis. The velocity contour plots and the parameter $\beta(t)$, the ratio of flow velocity in y direction over that in x direction, to show the induced secondary flow . As shown, we have It is found that the oscillatory behaviour of the fluid flow is only related to the ω while the Debye-Hückel parameter only changes the amplitude of the velocity field. There is also a time dependent structure of boundary layer at higher rotational frequencies. It is found that when the Debye-Hückel parameter and the rotation parameter are high, $\beta(t)$ oscillates near 45 degree implying identical flow rates in x and y directions.

In the second part of this study, an analytical model has been presented to describe the dynamics of capillary filling using a viscous fluid containing spinning particles. Spinning particles generate additional viscosities in the filling process called spin and vortex viscosity. In this study, three different time stages have been found during the capillary filling: Inertia force dominated, visco-

inertial stage, and viscous dominated regions. The last two regions are mainly affected by the spinning particles. An increase in the spin viscosity leads to a decrease in the front position of the moving liquid. The same behavior is observed for the relationship between vortex viscosity and the front position. Besides, when vortex and spin viscosities decrease the viscous force decreases which is the main reason for enhancement of the penetration rate.

4.2. Future Directions

The future direction for this study could be considering different type of fluids, channels, and speeding levels in the analysis as follow:

1- Considering Non-Newtonian fluids in both modeling (i.e., in the rotating problem and the filling dynamic problem).
2- Considering different type of channels in the modeling. We could use converging diverging channels in the modeling for both problems.
3- Applying the acceleration to the first problem (the constant spend rotation problem).

References

[1] Squires, T. M., & Quake, S. R. (2005). Microfluidics: Fluid physics at the nanoliter scale. *Reviews of modern physics*, *77*(3), 977.

[2] Yang, R. J., Fu, L. M., & Lin, Y. C. (2001). Electroosmotic flow in microchannels. *Journal of colloid and interface science*, *239*(1), 98-105.

[3] Tuckerman, D. B. (1984). Heat-transfer microstructures for integrated circuits (No. UCRL-53515). LAWRENCE LIVERMORE NATIONAL LAB CA.

[4] Incropera, F. P. (1999). Liquid Cooling of Electronic Devices By Single-Phase Convection, John Wiley and Sons. Inc., New York.

[5] Ho, C. M., & Tai, Y. C. (1998). Micro-electro-mechanical-systems (MEMS) and fluid flows. Annual Review of Fluid Mechanics, 30(1), 579-612.

[6] Stone, H. A., Stroock, A. D., & Ajdari, A. (2004). Engineering flows in small devices: microfluidics toward a lab-on-a-chip. Annu. Rev. Fluid Mech., 36, 381-411.

[7] Whitesides, G. M. (2006). The origins and the future of microfluidics. Nature, 442(7101), 368-373.

[8] Karniadakis, G. E., & Beskok, A. Micro flows: fundamentals and simulation. 2002.

[9] Kirby, B. J. (2010). Micro-and nanoscale fluid mechanics: transport in microfluidic devices. Cambridge University Press.

[10] Blazej, R. G., Kumaresan, P., & Mathies, R. A. (2006). Microfabricated bioprocessor for integrated nanoliter-scale Sanger DNA sequencing. Proceedings of the National Academy of Sciences, 103(19), 7240-7245.

[11] Nguyen, N. T., Shaegh, S. A. M., Kashaninejad, N., & Phan, D. T. (2013). Design, fabrication and characterization of drug delivery systems based on lab-on-a-chip technology. Advanced drug delivery reviews, 65(11), 1403-1419.

[12] Vladisavljević, G. T., Khalid, N., Neves, M. A., Kuroiwa, T., Nakajima, M., Uemura, K., ... & Kobayashi, I. (2013). Industrial lab-on-a-chip: design, applications and scale-up for drug discovery and delivery. Advanced drug delivery reviews, 65(11), 1626-1663.

[13] Li, P. C., & Harrison, D. J. (1997). Transport, manipulation, and reaction of biological cells on-chip using electrokinetic effects. Analytical Chemistry, 69(8), 1564-1568.

[14] Yasui, T., Mohamadi, M. R., Kaji, N., Okamoto, Y., Tokeshi, M., & Baba, Y. (2011). Characterization of low viscosity polymer solutions for microchip electrophoresis of non-denatured proteins on plastic chips. Biomicrofluidics, 5(4), 044114.

[15] Rivet, C., Lee, H., Hirsch, A., Hamilton, S., & Lu, H. (2011). Microfluidics for medical diagnostics and biosensors. Chemical Engineering Science, 66(7), 1490-1507.

[16] Cady, N. C., Stelick, S., Kunnavakkam, M. V., & Batt, C. A. (2005). Real-time PCR detection of Listeria monocytogenes using an integrated microfluidics platform. Sensors and Actuators B: Chemical, 107(1), 332-341.

[17] Gascoyne, P., Satayavivad, J., & Ruchirawat, M. (2004). Microfluidic approaches to malaria detection. Acta tropica, 89(3), 357-369.

[18] Lantz, P. G., Al-Soud, W. A., Knutsson, R., Hahn-Hägerdal, B., & Rådström, P. (2000). Biotechnical use of polymerase chain reaction for microbiological analysis of biological samples. Biotechnology annual review, 5, 87-130.

[19] Nguyen, N. T. (2011). Micromixers: fundamentals, design and fabrication. William Andrew.

[20] Huang, K. R., Hong, Z. H., & Chang, J. S. (2014). Microfluidic mixing on application of traveling wave electroosmosis. European Journal of Mechanics-B/Fluids, 48, 153-164.

[21] Zohar, Y., Lee, S. Y. K., Lee, W. Y., Jiang, L., & Tong, P. (2002). Subsonic gas flow in a straight and uniform microchannel. Journal of Fluid Mechanics, 472, 125-151.

[22] Sui, Y., Teo, C. J., & Lee, P. S. (2012). Direct numerical simulation of fluid flow and heat transfer in periodic wavy channels with rectangular cross-sections. International Journal of Heat and Mass Transfer, 55(1), 73-88.

[23] Sui, Y., Teo, C. J., Lee, P. S., Chew, Y. T., & Shu, C. (2010). Fluid flow and heat transfer in wavy microchannels. International Journal of Heat and Mass Transfer, 53(13), 2760-2772.

[24] Zheng, Z., Fletcher, D. F., & Haynes, B. S. (2014). Transient laminar heat transfer simulations in periodic zigzag channels. International Journal of Heat and Mass Transfer, 71, 758-768.

[25] Madou, M., Zoval, J., Jia, G., Kido, H., Kim, J., & Kim, N. (2006). Lab on a CD. Annu. Rev. Biomed. Eng., 8, 601-628.

[26] Takashima, M. (1976). The effect of rotation on electrohydrodynamic instability. Canadian Journal of Physics, 54(3), 342-347.

[27] Chang, C. C., & Wang, C. Y. (2011). Rotating electro-osmotic flow over a plate or between two plates. Physical Review E, 84(5), 056320.

[28] Xie, Z. Y., & Jian, Y. J. (2014). Rotating electroosmotic flow of power-law fluids at high zeta potentials. Colloids and Surfaces A: Physicochemical and Engineering Aspects, 461, 231-239.

[29] Kim, D. S., & Kwon, T. H. (2006). Modeling, analysis and design of centrifugal force-driven transient filling flow into a circular microchannel. Microfluidics and Nanofluidics, 2(2), 125-140.

[30] Ducrée, J., Haeberle, S., Brenner, T., Glatzel, T., & Zengerle, R. (2006). Patterning of flow and mixing in rotating radial microchannels. Microfluidics and Nanofluidics, 2(2), 97-105.

[31] Brenner, T., Glatzel, T., Zengerle, R., & Ducrée, J. (2005). Frequency-dependent transversal flow control in centrifugal microfluidics. Lab on a Chip, 5(2), 146-150.

[32] Beskok, A., & Karniadakis, G. (2005). Microflows and Nanoflows: Fundamentals and Simulation. Interdisciplinary Applied Mathematics. Springer.

[33] Probstein, R. F. (2003). Physicochemical hydrodynamics: an introduction. John Wiley & Sons.

[34] Masliyah, J. H., & Bhattacharjee, S. (2006). Electrokinetic and colloid transport phenomena. John Wiley & Sons.

[35] Tsao, H. K. (2000). Electroosmotic flow through an annulus. Journal of colloid and interface science, 225(1), 247-250.

[36] Dutta, P., & Beskok, A. (2001). Analytical solution of time periodic electroosmotic flows: analogies to Stokes' second problem. Analytical Chemistry, 73(21), 5097-5102.

[37] Kang, Y., Yang, C., & Huang, X. (2002). Electroosmotic flow in a capillary annulus with high zeta potentials. Journal of colloid and interface science, 253(2), 285-294.

[38] Kang, Y., Yang, C., & Huang, X. (2002). Dynamic aspects of electroosmotic flow in a cylindrical microcapillary. International Journal of Engineering Science, 40(20), 2203-2221.

[39] Li-Ping, B., Yong-Jun, J., Long, C., Jie, S., Hai-Yan, Z., & Quan-Sheng, L. (2013). Time periodic electroosmotic flow of the generalized Maxwell fluids in a semicircular microchannel. Communications in Theoretical Physics, 59(5), 615.

[40] Arulanandam, S., & Li, D. (2000). Liquid transport in rectangular microchannels by electroosmotic pumping. Colloids and Surfaces A: Physicochemical and Engineering Aspects, 161(1), 89-102.

[41] Wu, Z. Q., Cao, X. D., Chen, L., Zhang, J. R., Xia, X. H., Fang, Q., & Chen, H. Y. (2010). Study on the influence of cross-sectional area and zeta potential on separation for hybrid-chip-based capillary electrophoresis using 3-D simulations. Electrophoresis, 31(22), 3665-3674.

[42] Jiménez, E. M., Escandón, J. P., & Bautista, O. E. (2015, July). Study of the Transient Electroosmotic Flow of Maxwell Fluids in Square Cross-Section Microchannels. In ASME 2015 13th International Conference on Nanochannels, Microchannels, and Minichannels collocated with the ASME 2015 International Technical Conference and

Exhibition on Packaging and Integration of Electronic and Photonic Microsystems (pp. V001T04A015-V001T04A015). American Society of Mechanical Engineers.

[43] Chang, S. H. (2009). Transient electro-osmotic flow in cylindrical microcapillaries containing salt-free medium. Biomicrofluidics, 3(1), 012802.

[44] Keh, H. J., & Tseng, H. C. (2001). Transient electrokinetic flow in fine capillaries. Journal of colloid and Interface Science, 242(2), 450-459.

[45] Burgreen, D., & Nakache, F. R. (1964). Electrokinetic flow in ultrafine capillary slits1. The Journal of Physical Chemistry, 68(5), 1084-1091.

[46] Patankar, N. A., & Hu, H. H. (1998). Numerical simulation of electroosmotic flow. Analytical Chemistry, 70(9), 1870-1881.

[47] Bianchi, F., Ferrigno, R., & Girault, H. H. (2000). Finite element simulation of an electroosmotic-driven flow division at a T-junction of microscale dimensions. Analytical Chemistry, 72(9), 1987-1993.

[48] Ajdari, A. (2001). Transverse electrokinetic and microfluidic effects in micropatterned channels: Lubrication analysis for slab geometries. Physical Review E, 65(1), 016301.

[49] Zhao, M., Wang, S., & Wei, S. (2013). Transient electro-osmotic flow of Oldroyd-B fluids in a straight pipe of circular cross section. Journal of Non-Newtonian Fluid Mechanics, 201, 135-139.

[50] Li, X. X., Yin, Z., Jian, Y. J., Chang, L., Su, J., & Liu, Q. S. (2012). Transient electro-osmotic flow of generalized Maxwell fluids through a microchannel. Journal of Non-Newtonian Fluid Mechanics, 187, 43-47.

[51] Schoch, R. B., Han, J., & Renaud, P. (2008). Transport phenomena in nanofluidics. Reviews of Modern Physics, 80(3), 839.

[52] Lucas, R. (1918). Ueber das Zeitgesetz des kapillaren Aufstiegs von Flüssigkeiten. Colloid & Polymer Science, 23(1), 15-22.

[53] Washburn, E. W. (1921). The dynamics of capillary flow. Physical review, 17(3), 273.

[54] Hamraoui, A., & Nylander, T. (2002). Analytical approach for the Lucas–Washburn equation. Journal of colloid and interface science, 250(2), 415-421.

[55] Chakraborty, S. (2007). Electroosmotically driven capillary transport of typical non-Newtonian biofluids in rectangular microchannels. Analytica Chimica Acta, 605(2), 175-184.

[56] Quéré, D. (1997). Inertial capillarity. EPL (Europhysics Letters), 39(5), 533.

[57] Fries, N., & Dreyer, M. (2008). An analytic solution of capillary rise restrained by gravity. Journal of colloid and interface science, 320(1), 259-263.

[58] Bosanquet, C. H. (1923). LV. On the flow of liquids into capillary tubes. The London, Edinburgh, and Dublin Philosophical Magazine and Journal of Science, 45(267), 525-531.

[59] Zhmud, B. V., Tiberg, F., & Hallstensson, K. (2000). Dynamics of capillary rise. Journal of Colloid and Interface Science, 228(2), 263-269.

[60] Tas, N. R., Haneveld, J., Jansen, H. V., Elwenspoek, M., & Van Den Berg, A. (2004). Capillary filling speed of water in nanochannels. Applied Physics Letters, 85(15), 3274-3276.

[61] Oh, J. M., Faez, T., de Beer, S., & Mugele, F. (2010). Capillarity-driven dynamics of water–alcohol mixtures in nanofluidic channels. Microfluidics and nanofluidics, 9(1), 123-129.

[62] Das, S., Waghmare, P. R., & Mitra, S. K. (2012). Early regimes of capillary filling. Physical Review E, 86(6), 067301.

[63] Kutana, A., & Giapis, K. P. (2006). Atomistic simulations of electrowetting in carbon nanotubes. Nano letters, 6(4), 656-661.

[64] Ichikawa, N., & Satoda, Y. (1994). Interface dynamics of capillary flow in a tube under negligible gravity condition. Journal of colloid and interface science, 162(2), 350-355.

[65] Dreyer, M., Delgado, A., & Path, H. J. (1994). Capillary rise of liquid between parallel plates under microgravity. Journal of Colloid and interface science, 163(1), 158-168.

[66] Joly, L. (2011). Capillary filling with giant liquid/solid slip: dynamics of water uptake by carbon nanotubes. The Journal of chemical physics, 135(21), 214705.

[67] Waghmare, P. R., & Mitra, S. K. (2012). A comprehensive theoretical model of capillary transport in rectangular microchannels. Microfluidics and nanofluidics, 12(1-4), 53-63.

[68] Martic, G., Gentner, F., Seveno, D., Coulon, D., De Coninck, J., & Blake, T. D. (2002). A molecular dynamics simulation of capillary imbibition. Langmuir, 18(21), 7971-7976.

[69] Joos, P., Van Remoortere, P., & Bracke, M. (1990). The kinetics of wetting in a capillary. *Journal of colloid and interface science*, *136*(1), 189-197.

[70] Digilov, R. M. (2008). Capillary rise of a non-Newtonian power law liquid: impact of the fluid rheology and dynamic contact angle. Langmuir, 24(23), 13663-13667.

[71] J. S. Hansen, P. J. Daivis, and B. D. Todd, Microfluid. Nanofluid. 6, 785 (2009).

[72] Dahler, J. S., & Scriven, L. E. (1961). Angular momentum of continua. Nature, 192, 36-37.

[73] Evans, D. J., & Streett, W. B. (1978). Transport properties of homonuclear diatomics: II. Dense fluids. Molecular Physics, 36(1), 161-176.

[74] Finlayson, B. A. (2013). Spin-up of ferrofluids: The impact of the spin viscosity and the Langevin function. Physics of Fluids (1994-present), 25(7), 073101.

[75] Felderhof, B. U. (2012). Collective motion in ferrofluids. In Journal of Physics: Conference Series (Vol. 392, No. 1, p. 012001). IOP Publishing.

[76] Condiff, D. W., & Dahler, J. S. (1964). Fluid mechanical aspects of antisymmetric stress. Physics of Fluids (1958-1988), 7(6), 842-854.

[77] V. M. Zaitsev and M. I. Shliomis, "Entrainment of ferromagnetic suspension by a rotating field," J. Appl. Mech. Tech. Phys. 10, 696 _1969_.

[78] Chen, J., Chu, M., Koulajian, K., Wu, X. Y., Giacca, A., & Sun, Y. (2009). A monolithic polymeric microdevice for pH-responsive drug delivery. Biomedical microdevices, 11(6), 1251-1257.

[79] Bhatta, D., Michel, A. A., Villalba, M. M., Emmerson, G. D., Sparrow, I. J. G., Perkins, E. A., ... & Cartwright, G. A. (2011). Optical microchip array biosensor for multiplexed detection of bio-hazardous agents. Biosensors and Bioelectronics, 30(1), 78-86.

[80] Wang, Y. C., Stevens, A. L., & Han, J. (2005). Million-fold preconcentration of proteins and peptides by nanofluidic filter. Analytical chemistry, 77(14), 4293-4299.

[81] Kim, S. J., Wang, Y. C., Lee, J. H., Jang, H., & Han, J. (2007). Concentration polarization and nonlinear electrokinetic flow near a nanofluidic channel. Physical review letters, 99(4), 044501.

[82] Kim, S. J., Li, L. D., & Han, J. (2009). Amplified electrokinetic response by concentration polarization near nanofluidic channel. Langmuir, 25(13), 7759-7765.

[83] Pu, Q., Yun, J., Temkin, H., & Liu, S. (2004). Ion-enrichment and ion-depletion effect of nanochannel structur

[84] Manz, A., Graber, N., & Widmer, H. Á. (1990). Miniaturized total chemical analysis systems: a novel concept for chemical sensing. Sensors and actuators B: Chemical, 1(1), 244-248.

[85] Levine, S., Marriott, J. R., Neale, G., & Epstein, N. (1975). Theory of electrokinetic flow in fine cylindrical capillaries at high zeta-potentials. Journal of Colloid and Interface Science, 52(1), 136-149.

[86] Hsu, J. P., Kao, C. Y., Tseng, S., & Chen, C. J. (2002). Electrokinetic flow through an elliptical microchannel: effects of aspect ratio and electrical boundary conditions. Journal of Colloid and Interface Science, 248(1), 176-184.

[87] Sheu, T. W., Huang, V. C., & Rani, H. P. (2008). Development of an electro-osmotic flow model to study the dynamic behaviour in human meridian. International journal for numerical methods in fluids, 56(6), 739-751.

[88] Das, S., & Chakraborty, S. (2006). Analytical solutions for velocity, temperature and concentration distribution in electroosmotic microchannel flows of a non-Newtonian bio-fluid. Analytica Chimica Acta, 559(1), 15-24.

[89] Duffy, D. C., Gillis, H. L., Lin, J., Sheppard, N. F., & Kellogg, G. J. (1999). Microfabricated centrifugal microfluidic systems: characterization and multiple enzymatic assays. Analytical Chemistry, 71(20), 4669-4678.

[90] Ng, C. O., & Qi, C. (2015, July). Electro-osmotic flow in a rotating rectangular microchannel. In Proc. R. Soc. A (Vol. 471, No. 2179, p. 20150200). The Royal Society.

[91] Fluri, K., Fitzpatrick, G., Chiem, N., & Harrison, D. J. (1996). Integrated capillary electrophoresis devices with an efficient postcolumn reactor in planar quartz and glass chips. Analytical Chemistry, 68(23), 4285-4290.

[92] Santiago, J. G. (2001). Electroosmotic flows in microchannels with finite inertial and pressure forces. Analytical Chemistry, 73(10), 2353-2365.

[93] Bruus, H. (2008). Theoretical Microfluidics. Department of Micro and Nanotechnology Technical University of Denmark.

[94] Dhinakaran, S., Afonso, A. M., Alves, M. A., & Pinho, F. T. (2010). Steady viscoelastic fluid flow between parallel plates under

electro-osmotic forces: Phan-Thien–Tanner model. Journal of colloid and interface science, 344(2), 513-520.

[95] Kornev, K. G., & Neimark, A. V. (2001). Spontaneous penetration of liquids into capillaries and porous membranes revisited. Journal of colloid and interface science, 235(1), 101-113.

[96] Srivastava, N., & Burns, M. A. (2006). Analysis of non-Newtonian liquids using a microfluidic capillary viscometer. Analytical chemistry, 78(5), 1690-1696.

[97] Lavi, B., Marmur, A., & Bachmann, J. (2008). Porous media characterization by the two-liquid method: effect of dynamic contact angle and inertia. Langmuir, 24(5), 1918-1923.

[98] Mondal, P. K., Ghosh, U., Bandopadhyay, A., DasGupta, D., & Chakraborty, S. (2013). Electric-field-driven contact-line dynamics of two immiscible fluids over chemically patterned surfaces in narrow confinements. Physical Review E, 88(2), 023022.

[99] Persson, F., Thamdrup, L. H., Mikkelsen, M. B. L., Jaarlgard, S. E., Skafte-Pedersen, P., Bruus, H., & Kristensen, A. (2007). Double thermal oxidation scheme for the fabrication of SiO2 nanochannels. Nanotechnology, 18(24), 245301.

[100] B. Der and V. Born, (1920).

[101] P. Groot, S. R. De; Mazur, Non-Equilibrium Thermodynamics (Dover Books on Physics) (Dover Publications, 2011).

[102] Grad, H. (1952). Statistical mechanics, thermodynamics, and fluid

dynamics of systems with an arbitrary number of integrals. Communications on Pure and Applied Mathematics, 5(4), 455-494.

[103] Joseph, S., & Aluru, N. R. (2008). Pumping of confined water in carbon nanotubes by rotation-translation coupling. Physical review letters, 101(6), 064502.

[104] Bonthuis, D. J., Horinek, D., Bocquet, L., & Netz, R. R. (2009). Electrohydraulic power conversion in planar nanochannels. Physical review letters, 103(14), 144503.

[105] Felderhof, B. U. (2011). Ferrohydrodynamic pumping of a ferrofluid or electrohydrodynamic pumping of a polar liquid through a planar duct. Physics of Fluids (1994-present), 23(4), 042001.

[106] Rosensweig, R. E. (2013). Ferrohydrodynamics. Courier Corporation.

[107] Chaves, A., Torres-Diaz, I., & Rinaldi, C. (2010). Flow of ferrofluid in an annular gap in a rotating magnetic field. Physics of Fluids (1994-present), 22(9), 092002.

[108] Feng, S., Graham, A. L., Abbott, J. R., & Brenner, H. (2006). Antisymmetric stresses in suspensions: vortex viscosity and energy dissipation. Journal of Fluid Mechanics, 563, 97-122.

[109] Felderhof, B. U. (2011). Entrainment by a rotating magnetic field of a ferrofluid contained in a cylinder. Physical Review E, 84(2), 026312.

[110] Bandopadhyay, A., Ghosh, U., & Chakraborty, S. (2014). Capillary filling dynamics of viscoelastic fluids. Physical Review E, 89(5),

053024.

[111] Hirschfelder, J. O., Curtiss, C. F., Bird, R. B., & Mayer, M. G. (1954). Molecular theory of gases and liquids (Vol. 26). New York: Wiley.

[112] Snider, R. F., & Lewchuk, K. S. (1967). Irreversible thermodynamics of a fluid system with spin. The Journal of Chemical Physics, 46(8), 3163-3172.

Appendix

Here we describe how to obtain Eq (2.5) from the definition of species conservation. We have assumed that $\tau_p \gg \tau_c$ therefore, we can simplify Eq (2.4) as $\nabla.\left(\nabla\psi^* - \frac{\varepsilon D}{\sigma h^2}\nabla\rho_f^*\right) = 0$.

Also, we will explain how to obtain Eq (3-2). First we have to apply the assumption of velocity on *x* direction, no external torque, and constant force. Taking these assumptions into Eq (3-2), we will easily obtain Eq (3-4). Differentiating the second equation (3.2) with respect to *x*, and eliminating ω with the aid of the first equation, one derives a fourth order differential equation for velocity as: $\mathcal{L}(\mathcal{L}v_z - \kappa^2 v_z) = \frac{1}{2\eta_e}\mathcal{L}(-2F) + \frac{\kappa^2}{\eta}F$. Its solution takes the form:

$v_z = U + V(x) + X\ \cosh(\kappa x)$-$\frac{\zeta}{2\eta\eta_e\kappa}\left[e^{\kappa x}\int_x^h e^{-\kappa x'}Fdx' + e^{-\kappa x}\int_{-h}^x e^{\kappa x'}Fdx'\right]$. Here the function V(x) is given by $V(x) = \frac{1}{\eta}\int_x^h\int_0^{x'}Fdx'dx''$. The velocity U follows as: U = $-X\cosh(\kappa h) - Ze^{-\kappa h}$ and

Z=$\frac{\zeta}{\eta\eta_e\kappa}\int_0^h Fdx\cos h(\kappa x)\,dx.\int_x^h e^{-\kappa x'}Fdx'$.